Journal of the Mechanics and Physics of Solids 135 (2020) 103787

Contents lists available at ScienceDirect

Journal of the Mechanics and Physics of Solids

journal homepage: www.elsevier.com/locate/jmps

Self-assembly on a lipid membrane viewed as a first passage time problem

Xinyu Liao[a], Prashant K. Purohit[a,b,*]

[a] Graduate Group in Applied Mathematics and Computational Science, University of Pennsylvania, Philadelphia, PA 19104, USA
[b] Department of Mechanical Engineering and Applied Mechanics, University of Pennsylvania, Philadelphia, PA 19104, USA

ARTICLE INFO

Article history:
Received 26 August 2019
Revised 11 November 2019
Accepted 12 November 2019
Available online 14 November 2019

Keywords:
Lipid membrane
Inclusions
Self-assembly
Fokker-Planck equation

ABSTRACT

Lipid membranes form the outer covering of all biological cells. Embedded on the lipid membrane are numerous proteins that can diffuse on its surface due to its fluid nature. The proteins can also interact with each other through elastic and entropic forces that have their origin in the membrane's resistance to bending deformations. These interactions can be attractive or repulsive, and they likely play a role in self-assembly of proteins on the surface of the membrane to form scaffolds for exo- and endo-cytosis and also viruses. Thus, it is crucial to understand these elastic and entropic forces in detail and how they affect self-assembly of inclusions on the surface of membranes. Although most analyses of these phenomena utilize various simulation techniques, we use a semi-analytical method based on Gaussian integrals to compute the elastic and entropic interactions of inclusions. Once we have determined the interaction forces between inclusions, we use Langevin dynamics to study how they diffuse under the influence of these interaction forces. We focus first on two inclusions and cast their self-assembly as a first passage time problem. We show that an analytical treatment of the first passage time problem starting from a Fokker-Planck equation leads to a partial differential equation that can be solved numerically, and gives results which are in excellent agreement with the first passage time estimated from Langevin dynamics simulations. We are also able to account for hydrodynamic interactions between inclusions and show that they speed up the self-assembly. Finally, we use these insights to study how interaction forces influence the self-assembly of more than two inclusions. Our methods provide a different view of self-assembly that could be utilized for developing more advanced and efficient computational techniques.

1. Introduction

Interactions between inclusions on lipid membranes and their self-assembly leads to a host of biologically important functions such as budding of endo- and exo-cytotic vesicles, pore formation and assembly of viruses. These interactions could be curvature mediated (Golestanian et al., 1996; Kim et al., 1998a), membrane thickness mediated (Kahraman et al., 2016), entropic (Golestanian et al., 1996; Yolcu et al., 2014a) and even electrostatic (Lindgren et al., 2018). There is a large literature spanning a few decades on such interaction problems on membranes (Agrawal et al., 2016; Golestanian et al., 1996; Huang et al., 2011; Kahraman et al., 2016; Kim et al., 1998a; Li and Lykotrafitis, 2015; Müller and Deserno, 2010;

* Corresponding author at: Department of Mechanical Engineering and Applied Mechanics, University of Pennsylvania, Philadelphia, PA 19104, USA.
E-mail addresses: xinyul@sas.upenn.edu (X. Liao), purohit@seas.upenn.edu (P.K. Purohit).

https://doi.org/10.1016/j.jmps.2019.103787
0022-5096/

Ruiz-Herrero and Hagan, 2015; Schweitzer and Kozlov, 2015; Yolcu et al., 2014a; 2011). There is a smaller literature exploring the dynamics of self-assembly on lipid membranes (Matthews and Likos, 2013; Reynwar et al., 2007a; Ruiz-Herrero and Hagan, 2015), including continuum models (Arroyo et al., 2018; Tozzi et al., 2019). Most papers on dynamics of self-assembly assume phenomenological forms for the interactions between particles, rather than computing them from membrane deformations; this is because it is computationally expensive to do so. Many of these simulations have focused on the assembly of viruses on the surface of membranes due its relevance to disease and to the technologically important problem of drug delivery using nano-containers (Matthews and Likos, 2013; Ruiz-Herrero and Hagan, 2015). As such, the focus on these papers is on determining the conditions that lead to the assembly of full (virus) particles from the inclusions, but they say little about how the interaction forces between inclusions affect the time to assembly. However, an experimental paper by Shnyrova et al. (2007) shows that self-assembly of spherical buds formed by self-assembly of a viral protein occurs on the time scale of few seconds on vesicles that are a few microns in diameter (Shnyrova et al., 2007). Shnyrova et al. show using experiments that the interactions between these viral proteins are non-electrostatic, but the proteins induce local curvature of the membrane.

We have shown previously using a coarse-grained model that we can recover asymptotic forms for the curvature mediated elastic and entropic interactions of inclusions on membranes (Liang and Purohit, 2016; 2018). In particular, we had assumed that the inclusions were rigid, and hence had not accounted for the Gaussian curvature following arguments in (Kim et al., 1998b). However, the $1/r^4$ asymptotic form for the entropic interactions for circular inclusions separated by distance r on a lipid membrane happens to hold even if the inclusions are not rigid as shown by Lin et al. (2011). In fact, Lin et al. recover the $1/r^4$ dependence even in the presence of line tension at the inclusion-membrane interface. Another point to note is that Lin et al. (2011) showed that the inclusions' shape and mechanical properties enter the calculation of the fluctuation induced forces through a characteristic matrix. In our computations too the inclusions' shape and mechanical properties enter through a single 'stiffness' matrix. The general idea behind the calculation of fluctuation induced interaction forces is exactly the same in our work and that of Lin et al. (2011) (i.e., quadratic energies and Gaussian integrals for computing the partition function), except they do it analytically, while we compute the fluctuation determinants numerically. Thus, although we will stick with the simpler case of rigid inclusions in this work the paper of Lin et al. (2011) shows that our methods can be extended to compliant inclusions as well.

An important result in (Liang and Purohit, 2018) was that for rigid circular inclusions the competition of repulsive elastic forces and attractive entropic forces could lead to a maximum in the interaction free energy. The presence of a maximum indicates that at small separations there are attractive forces between inclusions which should lead to self-assembly. We had not demonstrated this self-assembly earlier since our coarse-grained model based on Gaussian integrals (Zhang and Crothers, 2003) was for equilibrium only. Here we go beyond equilibrium by combining our computational method with Langevin dynamic simulations to model the evolution of the membrane-inclusion system. Unlike most other papers on dynamic self-assembly our focus is not on particle and membrane shape which can be easily visualized through our calculations; rather, we are interested in the time to self-assembly for a few inclusions diffusing on a lipid membrane. We do not assume phenomenological forms for the interactions between inclusions; instead, we compute these interaction forces on the fly from membrane deformations caused by the boundary conditions imposed by the inclusions. We also take account of hydrodynamic interactions between inclusions which are known to speed up self-assembly (Matthews and Likos, 2013). Since most inclusions may not be circular we study the self-assembly of elliptical inclusions in this paper and show that their time to assembly is of the same order as that for circular inclusions of similar size.

An advantage of using Langevin dynamics combined with known asymptotic forms of the interaction energy between two inclusions is that we can invoke the Fokker-Planck equation to understand the evolution of the system. This allows us to make analytical progress with the problem of self-assembly instead of relying entirely on computations. If we fix one of the two inclusions at the center of the lipid membrane while allowing the other to diffuse under the action of the elastic and entropic forces then the time for coalescence of the two inclusions can be cast as a first passage time problem. For some special boundary conditions we can derive a differential equation for the first passage time starting from the Fokker-Planck equation. This allows us to verify our Langevin dynamic simulations against solutions from partial differential equations. To the best of our knowledge, such an exercise has not been attempted in the literature on self-assembly of inclusions on membranes. We show that our analytical techniques based on partial differential equations give reliable results much quicker than Langevin dynamic simulations.

In the remainder of the paper we first focus on circular inclusions in Section 2. We show the correspondence between the Langevin dynamics and Fokker-Planck equation based approaches. Then, in Section 3 we extend our analysis to elliptical inclusions; we compute the elastic and entropic interaction forces between them and again demonstrate the correspondence of the Langevin dynamics and Fokker-Planck equation based approaches. This section illustrates the generality of our approach since the problem is not radially symmetric when the inclusions are elliptical. In Section 4 we go back to circular inclusions, but we account for hydrodynamic interactions between them. We show yet again that the Langevin dynamics and Fokker-Planck equation based approaches give identical results. In Section 5 we analyze the self-assembly of multiple inclusions using Langevin dynamics and show the role of interaction forces at small separations. Finally, we conclude the paper with a brief summary of results.

2. Self-assembly of two circular inclusions in a lipid membrane

In this section we study the self-assembly of two circular inclusions on a square lipid membrane of finite size. We assume that one inclusion is fixed at the center of the membrane and the other is diffusing around driven by the entropic and elastic forces of interaction and due to Brownian motion. We cast the self-assembly of these two inclusions as a 'first passage time' problem within the theory of stochastic processes (Gillespie, 1991). Our expectation is that the elastic and entropic interactions between inclusions will affect this first passage time and determine the rate at which self-assembly occurs.

2.1. Energy landscape

It is well known that inclusions on lipid membranes interact via elastic and entropic forces (Golestanian et al., 1996; Hanlumyuang et al., 2014; Liang and Purohit, 2016; 2018; Lin et al., 2011; Reynwar et al., 2007b). Asymptotic forms of these interactions are available for circular inclusions (Reynwar et al., 2007b). It is understood that entropy (or fluctuations) is dominant at large separations (between inclusions), while the elastic force plays a bigger role at small separations. This could yield a maximum in the free energy at a critical separation (Liang and Purohit, 2018). Asymptotically, the entropic and elastic energy can be both written as (Golestanian et al., 1996; Reynwar et al., 2007b),

$$E_{\mathrm{el}}(r) = \frac{a_{\mathrm{el}}}{r^4} + O\left(\frac{1}{r^6}\right) \tag{1}$$

$$E_{\mathrm{en}}(r) = \frac{a_{\mathrm{en}}}{r^4} + O\left(\frac{1}{r^6}\right), \tag{2}$$

where r is distance between two rigid circular inclusions on a lipid membrane. a_{el} scales linearly with the bending modulus of the membrane and quadratically with the radius of each inclusion and the contact angle λ between the inclusion and the membrane for small contact angles; a_{en} scales linearly with the thermal energy scale k_BT (where k_B is the Boltzmann constant and T is absolute temperature) and quadratically with the radius of each inclusion. These dependencies have been computed anlaytically (Reynwar et al., 2007b) and verified numerically using a method based on Gaussian integrals (Ahmadpoor and Sharma, 2016; Liang and Purohit, 2016; 2018).

In Fig. 1 we choose a small contact angle $\lambda = 0.1$ radian, membrane bending modulus $K_b = 20k_BT$, and $T = 300$ K (at which $k_BT = 4.1$ pNnm) to plot the free energy for two inclusions on a membrane of dimensions 500 nm $\times$ 500 nm. Due to the limitations of our finite difference grid we can only have inclusions that are hexagonal in shape, so we choose two inclusions whose 'radii' are $R_1 = R_2 = 2l = 5$ nm, where $l = 2.5$ nm is the length of one equilateral triangle in Fig. 1. We choose various angles ψ_c between the line joining the center of the inclusions and the x_1-axis and plot the free energy of the membrane and inclusions as a function of the distance r separating the centers of the inclusions following methods described in (Liang and Purohit, 2018). We see that the free energy profile is mostly independent of ψ_c and depends only on r, as expected for circular inclusions on an infinite membrane. The slight dependence on the angle ψ_c arises due to the finite size of our membrane as well as the non-circular shape of both the membrane and inclusions among other causes (Liang and Purohit, 2018). The free energy has a maximum around $\frac{r}{l} = 20$ which corresponds to $r = 50$ nm and it decreases steeply for $\frac{r}{l} < 20$, while it is relatively flat for $\frac{r}{l} > 20$. Thus, an attractive force acts on the inclusions if the distance between them is smaller than a critical value which should lead to self-assembly. Here we note that when the center to center distance of two inclusions is small, typically $\frac{r}{l} < 6$, the formula Eqs. (1)–(2) given in (Reynwar et al., 2007b) may not fit the results from our finite difference calculations. Keeping these limitations in mind, we will analyze the self-assembly process in the following.

2.2. Langevin dynamics

The motion of an inclusion on a membrane is driven both by the elastic and entropic interactions given above and due to Brownian motion (or diffusion). The inclusions are small enough that the motion can be considered over-damped. We use Langevin dynamics to study the stochastic process of a diffusing inclusion driven by entropic and elastic forces and Brownian motion. The Langevin equation for the motion of a single inclusion is,

$$\frac{dr_i}{dt} = u_i, \tag{3}$$

$$m\frac{du_i}{dt} = -\nu u_i - \frac{\partial \phi}{\partial r_i} + \eta_i(t), \tag{4}$$

where r_i is the ith component of the position vector of the inclusion, u_i is ith component of the velocity vector, ν is translational drag coefficient, ϕ is the potential representing elastic and entropic interactions, m is the mass of the inclusion and $\eta_i(t)$ is a random force tensor with the following properties,

$$\langle \eta_i(t) \rangle = 0, \quad \langle \eta_i(t)\eta_j(t') \rangle = 2\nu k_B T \delta_{ij} \delta(t - t'), \tag{5}$$

We note here that the notation of any variables can also be regarded as a function of position in polar coordinates (E.g. ϕ refers to both the potential itself and a function of r and θ : $\phi = \phi(r, \theta)$). Since the mass of the inclusion is very small, we set LHS of Eq. (4) to zero. Then, after approximating the delta-correlated random noise term (Gillespie, 1991), we get,

$$dr_i = -\frac{1}{\nu}\frac{\partial \phi}{\partial r_i}dt + \sqrt{\frac{2k_BTdt}{\nu}}\xi_i, \tag{6}$$

where $\xi_i \sim \mathcal{N}(0, 1)$, a normally distributed random variable with mean 0 and variance 1. The translational drag coefficient ν of a circular inclusion is given by the SaffmanDelbrck model (Saffman and Delbrück, 1975),

$$\nu = \frac{4\pi\eta_m}{\log(2\epsilon^{-1}) - \gamma}, \tag{7}$$

where $\eta_m = 15.3 \times 10^{-9}$ Pa $\cdot$ s $\cdot$ m is the membrane viscosity (2D), $\eta_w = 8.5 \times 10^{-4}$ Pa $\cdot$ s is the bulk viscosity of water (3D), $l = 2.5$ nm is the radius of the circular cross section of the inclusion, $\epsilon = 2\eta_w l/\eta_m$ and $\gamma \approx 0.577$ is Euler's constant (Hormel et al., 2014). Arroyo and DeSimone (2009) calculated that for a lipid membrane of size about 500 nm membrane bending resistance and in-plane viscosity are the dominant driving and dissipative mechanisms. Here, membrane viscosity plays a crucial role in the dynamics of inclusions diffusing on a lipid membrane.

Our goal in doing the Langevin dynamic calculations is to determine the average time taken by the diffusing inclusion to coalesce with the stationary inclusion at the center of the membrane. This average time is usually referred to as a 'first passage time' in the literature of stochastic processes (Gillespie, 1991). We aim to determine this first passage time as a function of the initial distance r between the inclusions.

2.3. Fokker-Planck equation

Every Langevin equation can be represented by a Fokker-Planck equation (Gillespie, 1991). We use the Fokker-Planck equation to study the first passage time of the diffusing inclusion because this problem is analytically tractable. Recall that we consider two circular inclusions with radius $2l$ embedded in a square lipid membrane of side $2R_2$. One inclusion is fixed at the center $r = 0$ and the other is moving around. The diffusion coefficient is a scalar constant since the circular inclusion is isotropic and the lipid membrane is also isotropic. Then, the corresponding two-dimensional Fokker-Planck equation is a parabolic partial differential equation in radial symmetry and has a simple form,

$$\frac{\partial P}{\partial t} = -\nabla \cdot (\mathbf{f}P) + D\Delta P, \tag{8}$$

where $\mathbf{f} = -\frac{1}{\nu}\frac{\partial \phi}{\partial r}\mathbf{e_r}$ is the drift velocity and $\mathbf{e_r}$ is the unit vector in the radial direction (positive outward) and $P(r, t|y) = \int_0^{2\pi} p(r, t, \theta|y, \alpha)d\theta$ represents the probability density for a particle to be found at position r at time t in which p denotes the probability density at position r and angle θ given initial condition $r = y, \theta = \alpha$. Note that P is independent of α and is only dependent on y. Using the fact that $\Delta = \nabla \cdot \nabla$, Eq. (8) can be rewritten as a conservation law:

$$\frac{\partial P}{\partial t} = -\nabla \cdot (\mathbf{f}P) + D\nabla \cdot \nabla P = \nabla \cdot \left(\frac{1}{\nu}\frac{\partial \phi}{\partial r}P\mathbf{e_r} + D\nabla P\right) = \nabla \cdot \left[\left(\frac{1}{\nu}\frac{\partial \phi}{\partial r}P + D\frac{\partial P}{\partial r}\right)\mathbf{e_r}\right] = \nabla \cdot \mathbf{J}, \tag{9}$$

where $\mathbf{J} = \left(\frac{1}{\nu}\frac{\partial \phi}{\partial r}P + D\frac{\partial P}{\partial r}\right)\mathbf{e_r}$ is the flux of the probability density. The initial condition for Eq. (8) is

$$P(r, 0|y) = \frac{1}{r}\delta(r - y). \tag{10}$$

The boundary condition for Eq. (8) could be absorbing boundary conditions or reflecting boundary conditions or a mix of the two.

2.4. Steady-state solution

In order to obtain a non-vanishing steady-state solution to the Fokker-Planck equation Eq. (8), we assume two reflecting boundary conditions. One of the inclusions can move freely, but it will be bounced back if it is sufficiently close to the fixed inclusion at the center (i.e. $r = R_1$) or the outer boundary (i.e. $r = R_2$, we assume the inclusion's movement is restricted to the inscribed circle (orange) of the square membrane (purple) in Fig. 2(d)). Then, the two reflecting boundary conditions are given by Risken (1996),

$$J_r(R_1, t) = 0, \quad J_r(R_2, t) = 0, \quad \forall t \geq 0. \tag{11}$$

Eq. (11) impiles that,

$$\left(\frac{1}{\nu}\frac{\partial \phi}{\partial r}P + D\frac{\partial P}{\partial r}\right)\Bigg|_{(R_2,t)} = 0 \tag{12}$$

$$\left(k_B T \frac{\partial P}{\partial r} + \frac{\partial \phi}{\partial r} P\right)\Big|_{(R_2,t)} = 0, \tag{13}$$

where the Nernst-Einstein relation $\nu D = k_B T$ (Pathria, 2011) has been used in Eq. (13) and ϕ is the free energy. The steady-state solution of this Fokker-Planck equation can be obtained by setting $\frac{\partial P}{\partial t} = 0$ in Eq. (8). Then, from Eq. (9) we get,

$$\frac{\partial J_r}{\partial r} + \frac{1}{r} J_r = 0 \Longrightarrow J_r = \frac{B}{r}, \tag{14}$$

which means,

$$\frac{\partial P}{\partial r} + \frac{1}{\nu D} \frac{\partial \phi}{\partial r} P = \frac{B}{Dr} \tag{15}$$

$$\text{or,} \quad k_B T \frac{\partial P}{\partial r} + \frac{\partial \phi}{\partial r} P = \frac{B k_B T}{Dr}, \tag{16}$$

where B is a constant with the same units as D. The steady-state solution can be solved from the first order linear ODE Eq. (15),

$$P(r) = \exp\left(-\frac{\phi}{k_B T}\right)\left[\int \exp\left(\frac{\phi}{k_B T}\right)\frac{B}{rD} dr + C\right], \tag{17}$$

where C is a constant. We set $t \to \infty$ in Eq. (13) and compare it with Eq. (16), then it immediately follows that $B = 0$. Then, Eq. (17) reduces to

$$P(r) = C \exp\left(-\frac{\phi(r)}{k_B T}\right). \tag{18}$$

This is nothing but the Boltzmann distribution expected from equilibrium statistical mechanics. If we take $\phi = \frac{A_1}{r^4} + \frac{A_2}{r^6}$ with some constants A_1, A_2, then C can be solved from the fact that the integral of the probability function in polar coordinates equals 1,

$$1 = \int_{R_1}^{R_2} C \exp\left(-\frac{\phi}{k_B T}\right) r dr = \frac{C}{2} \int_{R_1}^{R_2} \exp\left(-\frac{\frac{A_1}{r^4} + \frac{A_2}{r^6}}{k_B T}\right) dr^2 = \frac{C}{2} \int_{R_1^2}^{R_2^2} \exp\left(-\frac{A_1}{k_B T}\frac{1}{q^2} - \frac{A_2}{k_B T}\frac{1}{q^3}\right) dq, \tag{19}$$

where we have changed variables in the last step $q = r^2$. C can be numerically solved from Eq. (19).

We use MATLAB to solve Eq. (8) and compare the evolution of the solution with the steady-state solution Eq. (18) with $R_1 = 19.8$ nm and $R_2 = 224.9$ nm. The results in Fig. 2 show that the Langevin method shown in Fig. 2(a) can correctly predict the evolution of the probability function $P(r, t)$ (obtained from Eq. (8) and shown in Fig. 2(b)) to steady state. Fig. 2(c) implies that the system consisting of membrane and two inclusions equilibrates by $t = 0.2$ s since the steady state solution nearly matches the solution at $t = 0.2$ s.

2.5. First passage time

Now that we have shown agreement between the results from the Fokker-Planck equation and the corresponding Langevin equation, we can proceed to an analysis of the first passage time for the self-assembly of two inclusions. An inclusion will typically be attracted to another inclusion when they are sufficiently close to each other. Hence, we will use absorbing boundary conditions at the inner boundary $r = R_1$. At the outer boundary, $r = R_2$ we use reflecting boundary conditions, but it is not possible to arrive at an analytical estimate of the mean first passage time under this boundary condition. However, the problem of the first passage time can be analytically solved if we use two absorbing boundary conditions at both sides. So, we proceed first with this calculation since it allows us to verify our first passage time estimated from the Langevin dynamic calculations in a rigorous fashion. Later, we will use more realistic boundary conditions in the Langevin dynamic simulations to estimate the rate of self-assembly.

We rewrite the Fokker-Planck Eq. (8) in the following form under two absorbing boundary conditions,

$$\frac{\partial P}{\partial t} = \frac{\partial}{\partial r}\left[\frac{1}{\nu}\frac{\partial \phi}{\partial r} P + D\frac{\partial P}{\partial r}\right] + \frac{1}{r}\left[\frac{1}{\nu}\frac{\partial \phi}{\partial r} P + D\frac{\partial P}{\partial r}\right], \tag{20}$$

with Dirichlet boundary condition,

$$P(R_1, t) = 0, \quad P(R_2, t) = 0, \quad \forall t \geq 0. \tag{21}$$

Define the survival probability $S(y, t)$,

$$S(y, t) = \int_{R_1}^{R_2} P(r, t|y) r dr. \tag{22}$$

Then, the first passage time density can be given as,

$$f(y,t) = -\frac{\partial S(y,t)}{\partial t} = -\int_{R_1}^{R_2} \frac{\partial P(r,t|y)}{\partial t} r dr. \tag{23}$$

In (Itô et al., 1957), Itô constructed the fundamental soluton for partial differential equations of parabolic type under Dirichlet boundary condition Eq. (21) which also satisfies the initial condition Eq. (10) in our problem. The exponential form of the fundamental solution implies that $P(r, t|y)$ exponentially decays to equilibrium for each r. Then, $tP(r, t|y) \to 0$ as $t \to \infty$. We use Eq. (23) to compute the first moment of the first passage time $T_1(y)$,

$$T_1(y) = \int_0^\infty f(y,t) t dt = -\int_0^\infty \int_{R_1}^{R_2} \frac{\partial P(r,t|y)}{\partial t} r dr t dt = \int_{R_1}^{R_2} \int_0^\infty P(r,t|y) dt r dr = \int_{R_1}^{R_2} g_1(r,y) r dr, \tag{24}$$

where g_1 is defined by,

$$g_1(r,y) = \int_0^\infty P(r,t|y) dt. \tag{25}$$

Using some technical but standard methods from the theory of stochastic process for the first passage time (Gillespie, 1991; Risken, 1996), we can derive the following ODE for $T_1(y)$ (see Appendix A),

$$\frac{\partial^2 T_1(y)}{\partial y^2} + \left(-\frac{1}{k_B T} \frac{\partial \phi}{\partial y} + \frac{1}{y} \right) \frac{\partial T_1(y)}{\partial y} + \frac{1}{D} = 0, \tag{26}$$

with boundary conditions,

$$T_1(R_1) = 0, \quad T_1(R_2) = 0. \tag{27}$$

We have solved the above ODE for the mean first passage time (with two absorbing boundary conditions) and plotted it as the red curve in Fig. 3(a). The results for first passage time from Langevin dynamics is the blue curve in Fig. 3(a). We find that the agreement between the two methods is excellent, suggesting that our Langevin dynamic simulations are predictive. The slight difference between these two methods is caused by (a) the analytical expression for the free energy Eqs. (1)-(2) used in Eq. (26) is not accurate at small r, (b) we have to use the free energy of the nearest vertex of the triangular element to approximate the free energy of the moving particle at any time step (see Fig. 2(d), and (c) the gradient of the free energy is computed by a finite difference method. In fact, the distribution of first passage time in Fig. 3(a) changes sharply if R_1 is changed by a small amount in the region of $R_1 < 15$ nm. In Fig. 3(b) we change to reflecting boundary condition at $r = R_2$ and absorbing boundary condition at $r = R_1$ and plot the first passage time obtained from Langevin dynamics as a function of the distance between inclusions. This plot gives us an estimate of the time to self-assembly for two inclusions under elastic and entropic interactions alone. The time scale in Fig. 3(b) is approximately one magnitude higher than in Fig. 3(a), which shows that the moving inclusion can exit the membrane much more rapidly when there are two 'doors' than when there is only one 'door'. Shnyrova et al. (2007) have shown that the time to self-assembly of a spherical bud formed bv a viral protein on vesicles about 4μm in diameter is a few seconds. Our estimates for time to self-assembly in Fig. 3(b) are about an order of magnitude lower, but the dimensions of our membrane are also much smaller than the vesicles used in (Shnyrova et al., 2007). Thus, our estimates of the time to self-assembly are not unreasonable. Fig. 3(c) shows how $P(r, t)$ evolves under absorbing boundary condition at R_1 and reflecting boundary condition at R_2. As time progresses, we are more likely to find the moving particle in a small neighborhood of the inner boundary. As $t \to \infty$, the probability to find a particle exactly at $r = R_1$ will be 1. Fig. 3(d) plots the first passage time in the absence of Brownian motion ($T = 0$). The maximum in the curve near $y = 70$nm happens becuase the free energy of the membrane-inclusion system has a maximum at that separation. Thus, there is zero force acting on the inclusiion when it is located at $y \approx 70$nm, so that the time to coalescence should tend to infinity. However, due to a finite grid size we cannot resolve this and we get a maximum in the curve. The time scales in Fig. 3(a) and Fig. 3(d) show that Brownian motion plays a dominant role in the model problem we are studying. In addition, the first passage time is hardly changed by removing interaction force (i.e. setting $\phi = 0$, see Fig. 3(a) dashed line), showing again that Brownian motion plays a bigger role than interaction force in the self-assembly. The inset in Fig. 3(d) is a comparison of the first passage time with $T = 0$ (red curve) and $T \neq 0$ (blue curve). The intersection of the two curves implies that the interaction force comes into play at small separations while the stochastic force is more significant when two particles are far away from each other. In Fig. 3(a)–(c) we choose $R_1 = 19.84$ nm because the analytical expression for the free energy given in (Reynwar et al., 2007b) is not accurate at small separations. However, in Fig. 3(d) we choose a smaller $R_1 = 12$ nm in order to demonstrate the effect of entropic and elastic force when two inclusions are sufficiently close. This choice of R_1 is reasonable as we do not use the formula in (Reynwar et al., 2007b) to make a comparison in Fig. 3(d).

An advantage of Eq. (26) is that we can easily estimate the effects of changing various physical parameters on the first passage time (and hence the rate of self-assembly) without having to run lengthy Langevin dynamics simulations. For example, if we fix the temperature and increase diffusion coefficient D (or decrease ν), T_1 will decrease significantly. If we increase the bending modulus, T_1 will decrease because the attractive forces between the inclusions become stronger, but this is not a significant effect since the attractive forces come into play at short range while the problem is dominated by diffusion.

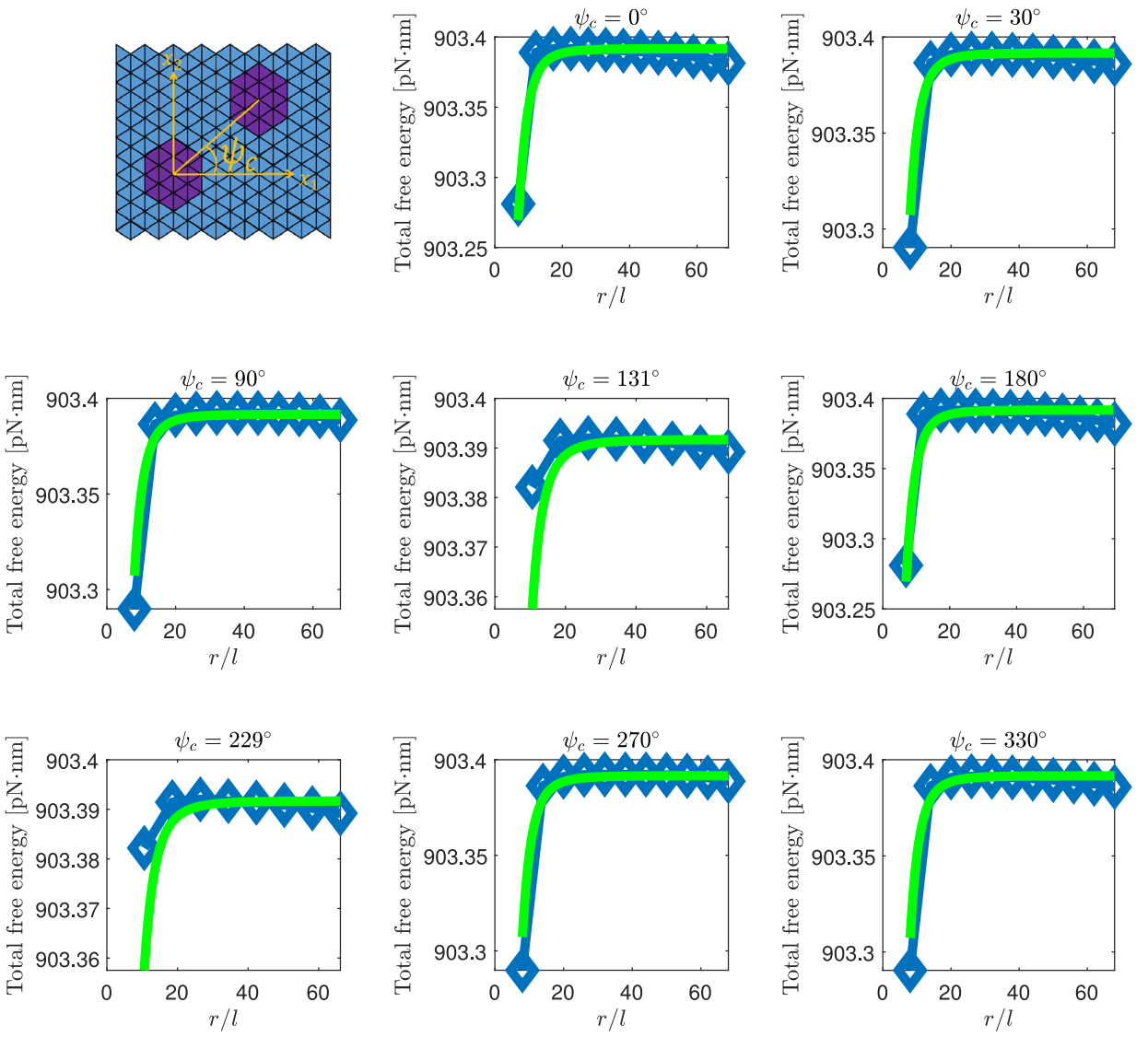

Fig. 1. Fitting of the total free energy by Eqs. (1) and (2). The panel on the top left shows two inclusions, one fixed at the center and the other located at (r, ψ_c) in a polar coordinate system. The remaining panels show the variation of the total free energy (elastic + entropic) of the membrane inclusion system as a function of r for various ψ_c. The symbols are obtained using our semi-analytic method based on Gaussian integrals (Liang and Purohit, 2018) and the lines are fits using Eqs. (1) and (2). The free energy is practically independent of ψ_c and depends only on r.

It is important to mention another subtle point. In computing the free energy of the membrane with two inclusions (i.e. $\phi(r)$) we are assuming equilibrium. This is a good assumption only if the longest wavelength vibration modes of the membrane have relaxed before an inclusion moves significantly. In (Lin and Brown, 2004), Lin and Brown computed the time over which the height correlation function $\langle w(t)w(0)\rangle/\langle w^2\rangle$ where w is the out-of-plane deflection of the neutral plane) goes to zero. For a flat square membrane of side 112 nm, this time is 25 μs (Lin and Brown, 2004). Since the relaxation time is proportional to L^3 where L is the side of the square membrane (Granek, 1997; Lin and Brown, 2004), the relaxation time in our problem can be computed as $25 \times 10^{-6} \times (500/112)^3 = 0.0022$ s, which is much smaller than the time scale in Fig. 3(a) and Fig. 3(b). Thus, by computing the free energy of the membrane-inclusion system and computing interaction forces from the gradient of the free energy we are 'coarse-graining' over the equilibrated vibration modes of the lipid membrane which allows us to focus entirely on the motion of the inclusions.

3. Self-assembly of elliptical inclusions

Our study of circular inclusions in the previous section showed that we can quantitatively describe their self-assembly on a lipid membrane. Most inclusions on a membrane (proteins involved in exo- and endo-cytosis, viral proteins) have more

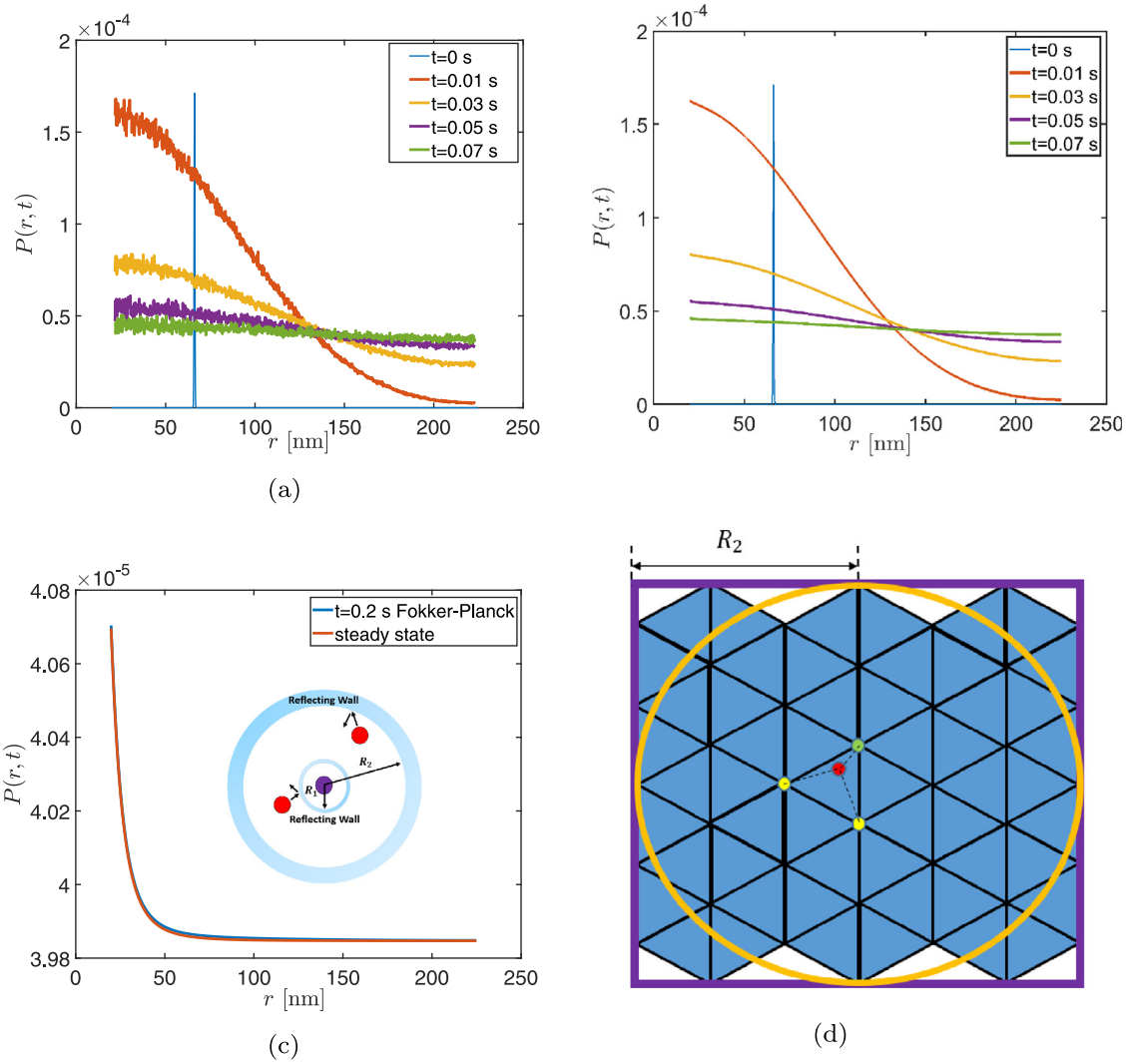

Fig. 2. The evolution of $P(r, t)$ to the steady state distribution Eq. (18). We divide the circular region into finitely many annulli with equal width Δr and run 8000 simulations at each fixed time. If s_j particles are found at the jth annulus, then $P(r_j, t)$ can be computed from the probability that a particle is found at the jth annulus: $P(r_j)r_j\Delta r = s_j/8000$. (a) $P(r, t)$ derived from Langevin dynamics. (b) $P(r, t)$ derived from Fokker-Planck equation. (c) Comparison between $P(r)$ at $t = 0.2$ s computed from Fokker-Planck equation and its steady state distribution. (d) Since we can compute the free energy only on a vertex of each triangular element, the free energy at the red point is approximated by the free energy at the green point. The orange circle shows the outer boundary $r = R_2$ for the first passage time problems studied next. (For interpretation of the references to colour in this figure legend, the reader is referred to the web version of this article.)

complex shapes (Kahraman et al., 2016). For this reason we consider inclusions with elliptic cross-section. Three types of ellipses '$\varphi_{\frac{\pi}{6}}$', '$\varphi_{\frac{\pi}{2}}$', '$\varphi_{\frac{5\pi}{6}}$' are considered here and are shown in Fig. 4(a). They differ by how they are oriented with respect to our triangular grid. Some analytical results are available for these inclusions that can be used to verify our computations.

3.1. Fitting of the interaciton free energy

Kwiecinski et al. (2019) proposed that the elastic energy of an infinite membrane with two identical elliptical inclusions depends on the inverse separation r squared to lowest order,

$$E_{\text{el}} = \frac{c_1(\cos 2\psi_{e1} + \cos 2\psi_{e2})}{r^2} + \frac{c_1'}{r^4}. \tag{28}$$

This result is derived assuming elastic deformations of the lipid membrane only. It depends on the orientation of the inclusions through the angles ψ_{e1} and ψ_{e2} as shown in figure Fig. 4(b). Note that while the elastic interaction between two circular inclusions is always repulsive, Kwiecinski et al. (2019) showed that one can have attractive interactions between

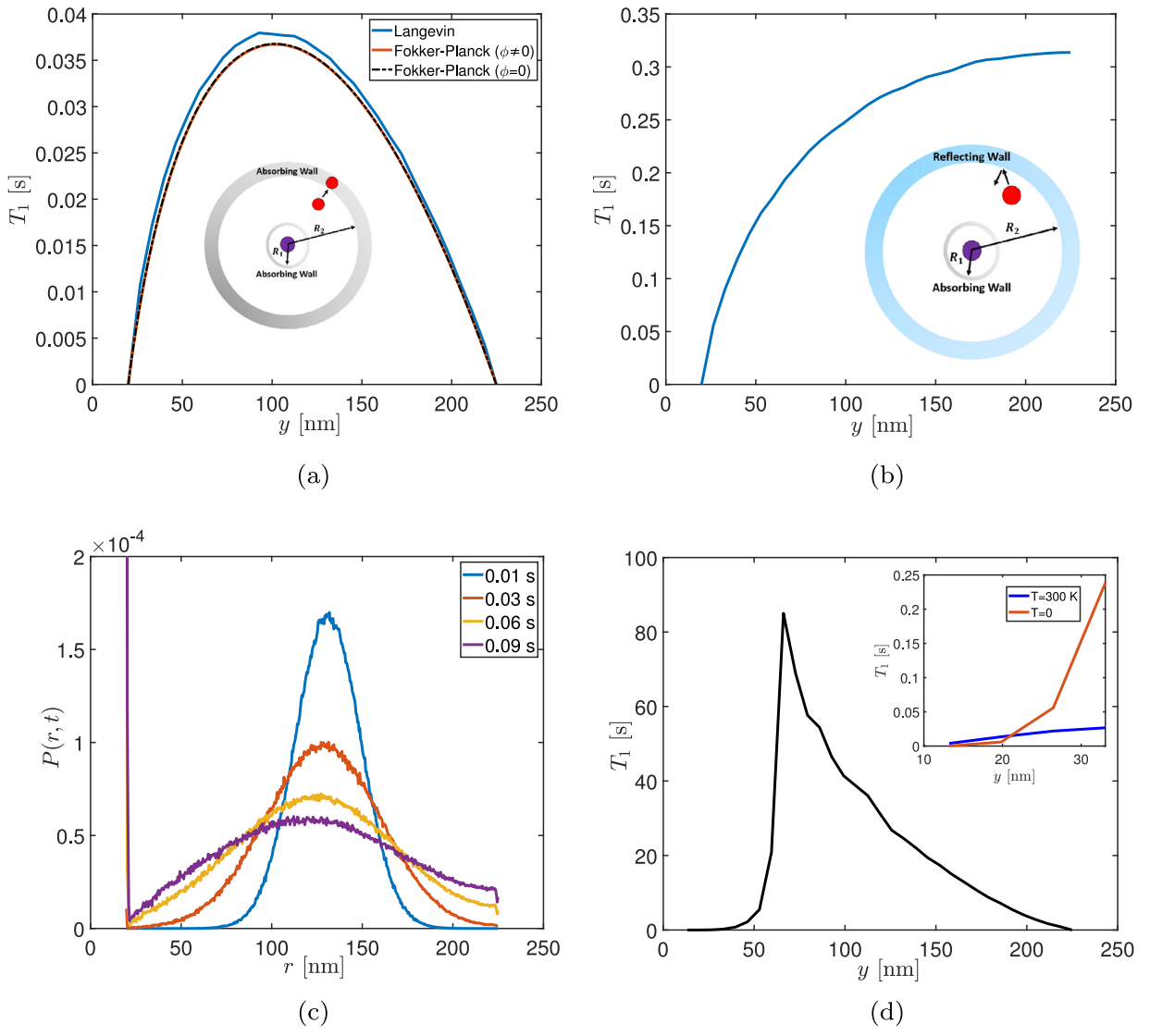

Fig. 3. (a) Comparison of the first passage time derived from Fokker-Planck equation and Langevin dynamics. The inset shows two absorbing boundary condition at $r = R_1$ and $r = R_2$. (b) Prediction of the first passage time using Langevin dynamics. The inset shows an absorbing boundary condition at R_1 and a reflecting boundary condition at R_2. (c) The evolution of $P(r, t|y)$. The moving particle starts its kinetics at $y = 132.3$ nm (around the middle). As time is progressing, the probability of the moving particle being absorbed to the inner absorbing wall increases. (d) The black curve describes the first passage time without thermal fluctuation ($T = 0$) at initial angle $\alpha = 49.1^\circ$. The first passage time should go to infinity at some point around 70 nm shown in this graph, which is close to the maximum point of the total free energy in Fig. 1. The inset is a comparison of the first passage time between $T = 300$ K and $T = 0$ at $\alpha = 49.1^\circ$.

elliptical inclusions even in the absence of thermal fluctuations. Thus, elliptical inclusions may have higher propensity to self-assembly.

The entropic interactions between elliptical inclusions have not been studied analytically, to the best of our knowledge. However, we can use our method based on Gaussian integrals to compute the entropic interactions (Liang and Purohit, 2018). We will use the form of expressions given in (Yolcu et al., 2014b) to fit a simple analytical expression to the entropic part of the free energy.

$$E_{\text{en}} = \frac{c_2'}{r^4} + \frac{c_3}{r^6} + O\left(\frac{1}{r^8}\right). \tag{29}$$

Ignoring $O\left(\frac{1}{r^8}\right)$, we get an approximate expression for the total free energy,

$$E = E_{\text{el}} + E_{\text{en}} = \frac{c_1(\cos 2\psi_{e1} + \cos 2\psi_{e2})}{r^2} + \frac{c_2}{r^4} + \frac{c_3}{r^6} + M(\varphi_\beta, \varphi_\eta), \tag{30}$$

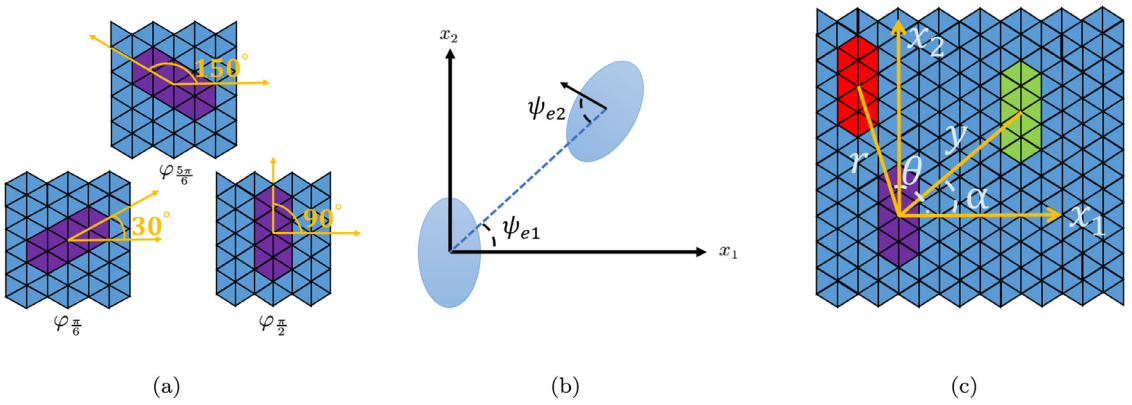

Fig. 4. (a) Three types of elliptical inclusions in the finite difference grid based on the semi-analytic Gaussian integral method proposed in (Liang and Purohit, 2016; 2018). (b) The interaction of two elliptical inclusions in a lipid membrane. ψ_{e1}, ψ_{e2} are angles between the line connecting their centers and the major axis of the two elliptical inclusions. (c) Elliptical inclusion moving on the membrane without rotating. The green one is the initial position (y, α) and the red one is the current position (r, θ) of the moving elliptical inclusion. The purple one is the fixed inclusion located at the center. (For interpretation of the references to colour in this figure legend, the reader is referred to the web version of this article.)

where $c_1, c_2, c_3, c_1', c_2'$ are constants and the function $M(\varphi_\beta, \varphi_\eta)$, $\eta, \beta \in \{\frac{\pi}{6}, \frac{\pi}{2}, \frac{5\pi}{6}\}$ coming from both the elastic part Eq. (28) and entropic part Eq. (29) depends on the orientations of the two elliptical inclusions, but not on r.

Our first objective is to determine whether Eq. (30) faithfully matches our computations based on the methods in (Liang and Purohit, 2016; 2018). We have a square membrane and we place an elliptical inclusion at its center. We then place a second elliptic inclusion at various other positions on the membrane and compute the elastic and entropic parts of the free energy of the membrane inclusion system. Fig. 5 shows that our method agrees reasonably with Eq. (30). However, the constants (c_1, c_2, c_3) fitted from Eq. (30) vary slightly among different quadrants (the major and minor axes of the ellipse in the center divides the square into four quadrants). This happens because we use triangular elements to mesh the square membrane which causes the mesh in each quadrant to be slightly different introducing some anisotropy. Also, we have a finite membrane while the analytical calculation in the elastic part of Eq. (30) assumes an infinite membrane (Kwiecinski et al., 2019). Nevertheless, in each quadrant Eq. (30) is able to fit the data from our numerical calculations quite well. We choose $\psi_e = \psi_{e1} = \psi_{e2}$. Our method captures the crossover from repulsive force at the smallest $\psi_e = 0^\circ$ to attractive force at the largest $\psi_e = 90^\circ$, which is likely to be important in studying the Brownian motion of anisotropic particles. The free energy function is fitted over all four quadrants since the analytical expression Eq. (30) will be used in the Fokker-Planck equation to compute the first passage time.

3.2. Langevin dynamics

When the inclusion is not circular, the translational drift (or drag) coefficient and diffusion coefficient should be characterized by second order tensors ν_{ij}, D_{ij} respectively where index $i, j = 1, 2$ represent two perpendicular directions x_1 and x_2. For an ellipsoid in 2D, the translational drift tensor is diagonal and described by ν_a, ν_b for motion parallel and perpendicular to its major axis (Han et al., 2006). It is understood that the ellipsoid would diffuse more rapidly along its major axis, and this could lead to rotational diffusion due to particle anisotropy (Han et al., 2006; Perrin, 1934; 1936). For simplicity, rotational diffusion of the inclusion is not considered in this subsection. The particle will diffuse along its major axis x_1 and minor axis x_2 independently with diffusion coefficient $D_\gamma = k_B T/\nu_\gamma$, for γ either a or b. To the best of our knowledge, many analytical expressions are available for the diffusion coefficient of ellipsoids in 3D, but little has been said about a cylindrical particle with elliptic cross section diffusing on a lipid membrane. Since we need diffusion and drag coefficients for such a particle on a lipid membrane, we combine the ideas of Saffman and Delbrück (1975), Han et al. (2009) to add a geometric factor into the SaffmanDelbrck model Eq. (7),

$$\nu_a = \frac{4\pi\eta_m}{\log(2\bar{\epsilon}^{-1}) - \gamma} G_a, \qquad \nu_b = \frac{4\pi\eta_m}{\log(2\bar{\epsilon}^{-1}) - \gamma} G_b, \tag{31}$$

where $G_a, \bar{\epsilon}, G_b$ are given by,

$$G_a = \frac{8}{3} \frac{1}{\left[\frac{2\Gamma}{1-\Gamma^2} + \frac{2\Gamma^2-1}{(\Gamma^2-1)^{\frac{3}{2}}} \log\left(\frac{\Gamma+\sqrt{\Gamma^2-1}}{\Gamma-\sqrt{\Gamma^2-1}}\right)\right]}, \quad \bar{\epsilon} = \frac{2\eta_w\sqrt{l_a l_b}}{\eta_m}, \quad G_b = \frac{8}{3} \frac{1}{\left[\frac{\Gamma}{\Gamma^2-1} + \frac{2\Gamma^2-3}{(\Gamma^2-1)^{\frac{3}{2}}} \log\left(\Gamma+\sqrt{\Gamma^2-1}\right)\right]}, \tag{32}$$

where l_a, l_b are length of major axis, minor axis respectively and $\Gamma = l_a/l_b$ is the ellipsoid aspect ratio. These expressions are not expected to be exact, but they do capture the anisotropic drag experienced by particles with elliptic cross-section.

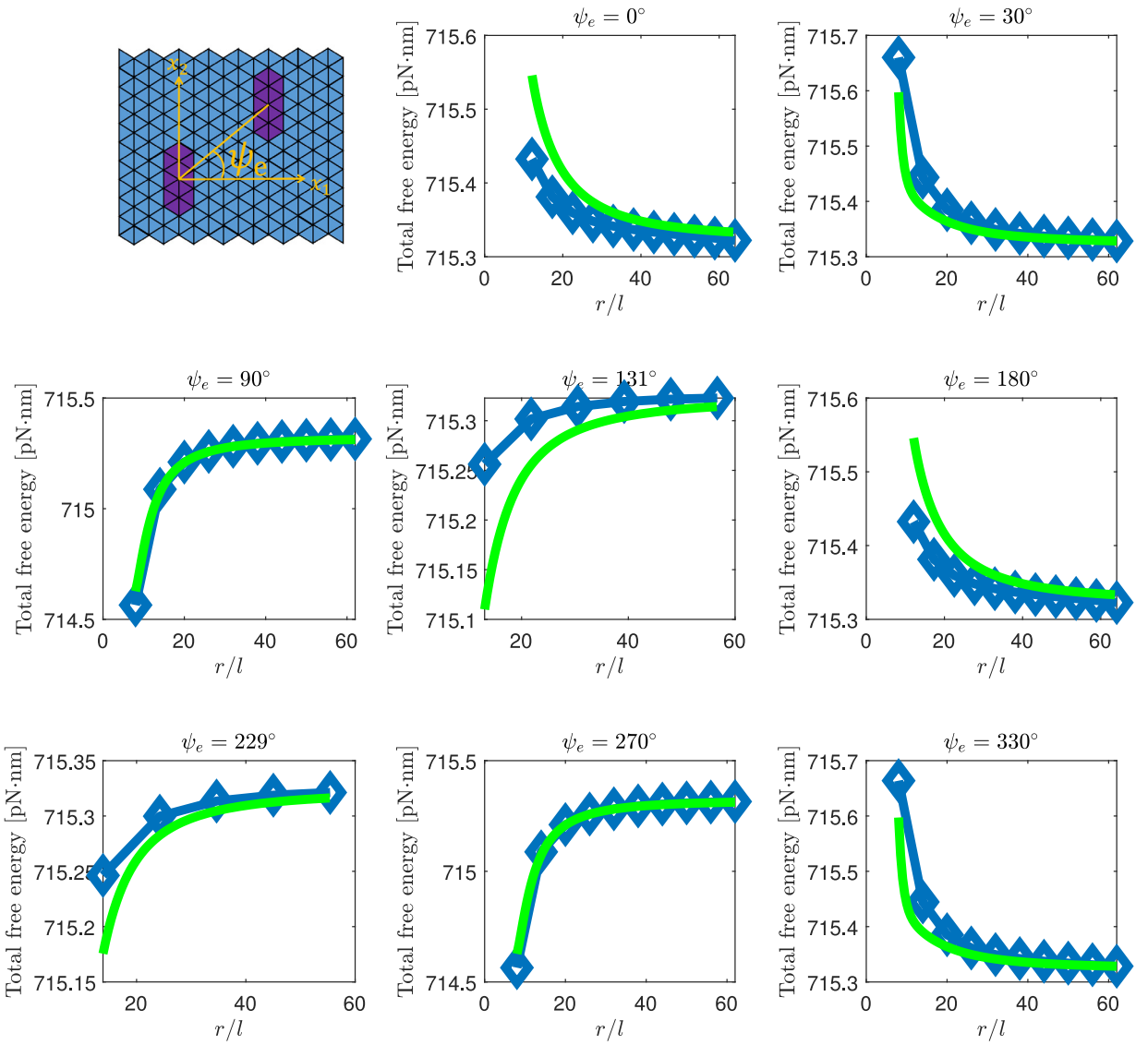

Fig. 5. Fitting of the total free energy by Eq. (30). The two elliptical inclusions are chosen to be type φ_{90} (see Fig. 4(a)) as shown in the panel on the top left. One inclusion is fixed at the center and the other is located at (r, ψ_c) in a polar coordinate system. The remaining panels show the variation of the total free energy (elastic + entropic) of the membrane-inclusion system as a function of r for various ψ_c. The symbols are obtained using our semi-analytic method based on Gaussian integrals (Liang and Purohit, 2018) and the lines are fits using Eq. (30). Note that some values of ψ_c result in repulsive interactions for small r (e.g. $\psi_c = 0°, 30°$), while others give an attractive interaction (e.g. $\psi_c = 90°, 270°$).

Then, the Langevin Eqs. (3), (4) are rewritten as,

$$\frac{dr_i}{dt} = u_i, \tag{33}$$

$$m\frac{du_i}{dt} = -\nu_{ij}u_j - \frac{\partial \phi}{\partial r_i} + \eta_i(t), \tag{34}$$

where $\eta_i(t)$ here has the following properties,

$$\langle \eta_i(t) \rangle = 0, \quad \langle \eta_i(t)\eta_j(t') \rangle = 2\nu_{ij}k_BT\delta(t-t'). \tag{35}$$

Accordingly, Eq. (6) is modified to,

$$dr_i = -\nu_{ij}^{-1}\frac{\partial \phi}{\partial r_j}dt + \sqrt{\frac{2k_BTdt}{\nu_{ii}}}\xi_i \text{ (no sum in the second term).} \tag{36}$$

3.3. Fokker-Planck equation

Since the inclusions are elliptical, P is dependent both on y and the angle α (see Fig. 4(c)), and the potential ϕ does not have radial symmetry. The drift velocity is accordingly also not isotropic. For these reasons, we consider p instead of P, and then the Fokker-Planck equation is a partial differential equation of parabolic type,

$$\begin{aligned}\frac{\partial p}{\partial t} &= \frac{\partial}{\partial x_i}\left[\nu_{ij}^{-1}\frac{\partial \phi}{\partial x_j}p\right] + \frac{\partial^2}{\partial x_i \partial x_j}\left[D_{ij}p\right] = -\left[-\frac{\partial}{\partial x_i}\left(D_{ij}\frac{\partial p}{\partial x_j}\right) - \left(\nu_{ij}^{-1}\frac{\partial \phi}{\partial x_j}\right)\frac{\partial p}{\partial x_i} - \frac{\partial}{\partial x_i}\left(\nu_{ij}^{-1}\frac{\partial \phi}{\partial x_j}\right)p\right] \\ &= \frac{1}{\nu_a}\left(\frac{\partial^2 \phi}{\partial x_1^2}p + \frac{\partial \phi}{\partial x_1}\frac{\partial p}{\partial x_1}\right) + \frac{1}{\nu_b}\left(\frac{\partial^2 \phi}{\partial x_2^2}p + \frac{\partial \phi}{\partial x_2}\frac{\partial p}{\partial x_2}\right) + D_a\frac{\partial^2 p}{\partial x_1^2} + D_b\frac{\partial^2 p}{\partial x_2^2}. \end{aligned} \tag{37}$$

3.4. First passage time

The first passage time of Eq. (24) can be redefined as,

$$T_1(y,\alpha) = \int_0^\infty f(y,\alpha,t)t dt = -\int_0^\infty \int_{R_1}^{R_2}\int_0^{2\pi} \frac{\partial p(r,\theta,t|y,\alpha)}{\partial t} r dr d\theta t dt \tag{38}$$

$$= \int_{R_1}^{R_2}\int_0^{2\pi}\int_0^\infty p(r,\theta,t|y,\alpha) dt d\theta r dr = \int_{R_1}^{R_2}\int_0^{2\pi} q_1(r,\theta|y,\alpha) d\theta r dr, \tag{39}$$

where we have used $tp(r, \theta, t|y, \alpha) \to 0$ as $t \to \infty$ in the first equation of the second line and q_1 is defined by,

$$q_1(r,\theta|y,\alpha) = \int_0^\infty p(r,\theta,t|y,\alpha) dt. \tag{40}$$

After some lengthy algebra (see Appendix B), we can derive a second order PDE for $T_1(y, \alpha)$:

$$\begin{aligned}&\left(D_a\cos^2\alpha + D_b\sin^2\alpha\right)\frac{\partial^2 T_1}{\partial y^2} + \left(D_a\frac{\sin^2\alpha}{y^2} + D_b\frac{\cos^2\alpha}{y^2}\right)\frac{\partial^2 T_1}{\partial \alpha^2} + \left(-D_a\frac{\sin 2\alpha}{y} + D_b\frac{\sin 2\alpha}{y}\right)\frac{\partial^2 T_1}{\partial y \partial \alpha} \\ &+ \left[D_a\frac{\sin^2\alpha}{y} + D_b\frac{\cos^2\alpha}{y} + \frac{1}{\nu_a}\left(\frac{\sin 2\alpha\frac{\partial \phi}{\partial \alpha}}{2y} - \cos^2\alpha\frac{\partial \phi}{\partial y}\right) - \frac{1}{\nu_b}\left(\frac{\sin 2\alpha\frac{\partial \phi}{\partial \alpha}}{2y} + \sin^2\alpha\frac{\partial \phi}{\partial y}\right)\right]\frac{\partial T_1}{\partial y} \\ &+ \left[D_a\frac{\sin 2\alpha}{y^2} - D_b\frac{\sin 2\alpha}{y^2} + \frac{1}{\nu_a}\left(\frac{\sin 2\alpha\frac{\partial \phi}{\partial y}}{2y} - \frac{\sin^2\alpha\frac{\partial \phi}{\partial \alpha}}{y^2}\right) - \frac{1}{\nu_b}\left(\frac{\sin 2\alpha\frac{\partial \phi}{\partial y}}{2y} + \frac{\cos^2\alpha\frac{\partial \phi}{\partial \alpha}}{y^2}\right)\right]\frac{\partial T_1}{\partial \alpha} + 1 = 0. \end{aligned} \tag{41}$$

Then, the first passage time solved from Eq. (41) by finite difference method (see Appendix C) can be compared with estimates from Langevin dynamics calculations as summarized in Fig. 6.

The excellent agreement between the two methods demonstrates that our ideas can be applied to anisotropic inclusions. The curves in Fig. 6(a) are not as smooth as those in Fig. 3(a) due to our finite difference grid, finite time step dt and our method to compute free energy (see Fig. 2(d)). Nevertheless, it shows that the first passage time depends on the initial orientation of the moving inclusion if the initial center to center distance is fixed. An interesting result of Fig. 6 is that the first passage time at initial angle 90° under any fixed y is the largest among the four cases while it has the strongest attractive entropic force in this direction (see Fig. 5). On the other hand, the moving inclusion is getting absorbed most rapidly at initial angle 0° even though the force in that direction is repulsive. This seems to contradict our intuition. In fact, if Brownian motion is prohibited by setting $T = 0$ in Eq. (36), the first passage time will be in the reverse order (i.e. T_1 at $\alpha = 90°$ is the smallest). The seeming anomaly in the presence of Brownian motion happens for the following reason. At $\alpha = 90°$, the free energy reaches a local minimum in the θ direction that looks like a 'trap'. It takes the moving particle more time to escape from this trap. By contrast, at $\alpha = 0°$, the free energy is monotonic along θ direction. As a consequence, the moving particle is more likely to move in only one direction, and therefore reaches either of the two 'doors' at $r = R_1, r = R_2$ in less time. Fig. 6(c) provides a prediction computed from Langevin dynamics under reflecting boundary condition at R_2 and absorbing boundary condition at R_1. The time scales are similar to those seen for circular inclusions in Fig. 3(c). The inset in Fig. 6(d) indicates similar results as in the circular case, i.e. interaction force comes into play at small separations, while Brownian motion plays a bigger role when the two inclusions are far from each other.

3.5. Rotational diffusion of elliptical inclusions

If the rotational effects of elliptical inclusions are considered, the translational diffusion tensor D_{ij} will be time-dependent (Han et al., 2006). Accordingly, the linear elliptic operator in Eq. (B.2) will be time-dependent, too. For this reason, a PDE for the first passage time like Eq. (41) cannot be derived from the Fokker-Planck equation. Nevertheless, we can still compute

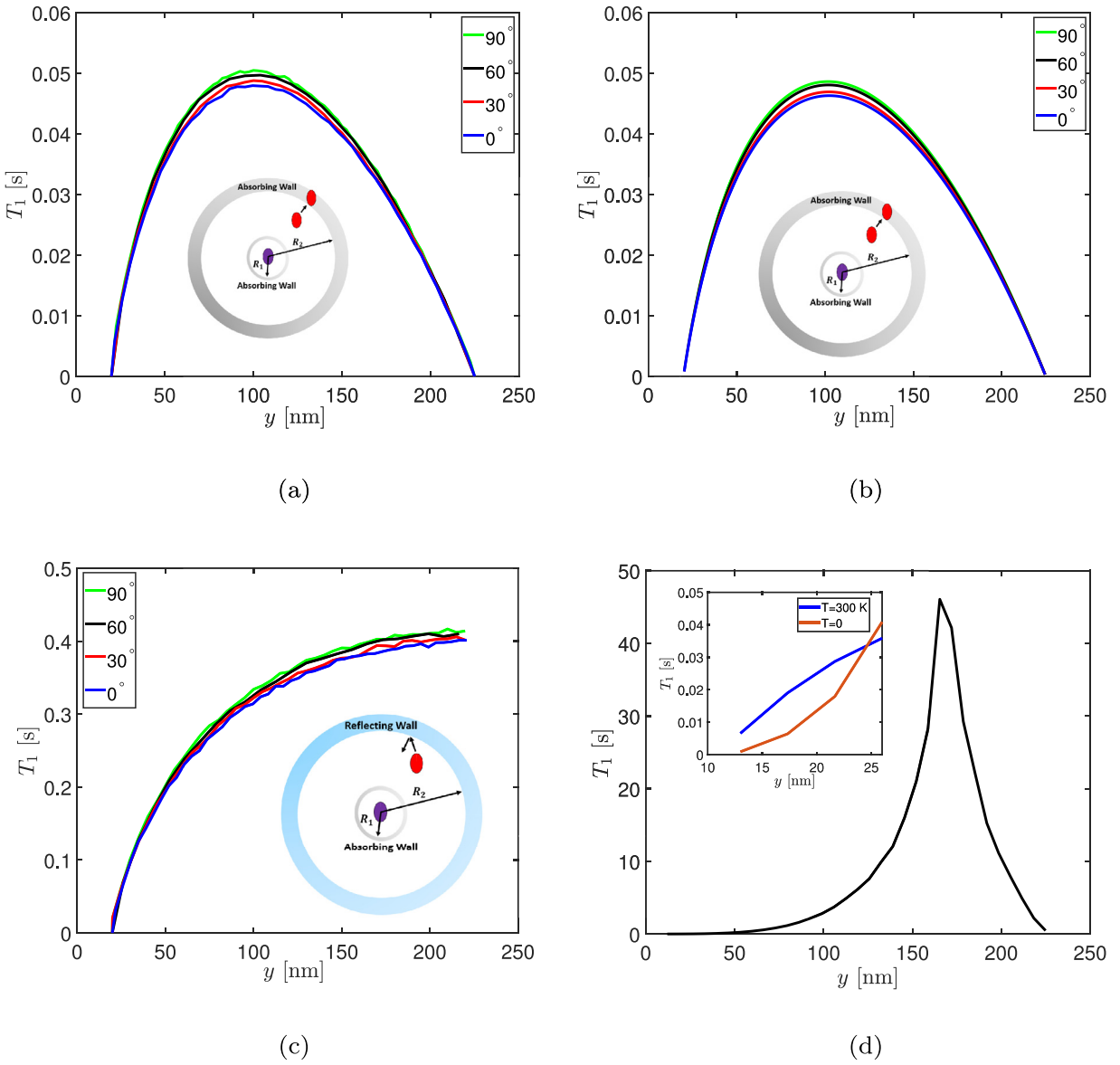

Fig. 6. The first passage time under different initial angle $\alpha = 90^\circ, 60^\circ, 30^\circ, 0^\circ$ derived from (a) Langevin dynamics and (b) Fokker-Planck equation. The insets of these two plots show two absorbing boundary conditions at $r = R_1$ and $r = R_2$. (c) gives a prediction using Langevin dynamics for a reflecting boundary condition at R_2 and an absorbing boundary condition at R_1 (as shown in the inset). (d) The black curve describes the first passage time without thermal fluctuation ($T = 0$) at $\alpha = 49.1^\circ$. The inset is a comparison of the first passage time between $T = 300$ K and $T = 0$ at $\alpha = 49.1^\circ$.

the first passage time from Langevin dynamics, which will now have an additional equation for the rotational motion of the elliptical inclusion (Han et al., 2006),

$$\frac{d\Theta}{dt} = \omega, \tag{42}$$

$$I\frac{d\omega}{dt} = -\nu_\theta \omega - \frac{\partial \phi}{\partial \Theta} + \eta_\theta(t), \tag{43}$$

where Θ is an angle (see Fig. 7(a)), ω is an angular velocity and I is a moment of inertia of the elliptical inclusion. ν_θ is a rotational drag coefficient, and $\eta_\theta(t)$ is a random torque given by Saffman and Delbrück (1975) and with the following properties,

$$\nu_\theta = 16\pi\eta_m l^2, \quad \langle \eta_\theta(t) \rangle = 0, \quad \langle \eta_\theta(t)\eta_\theta(t') \rangle = 2\nu_\theta k_B T \delta(t - t'). \tag{44}$$

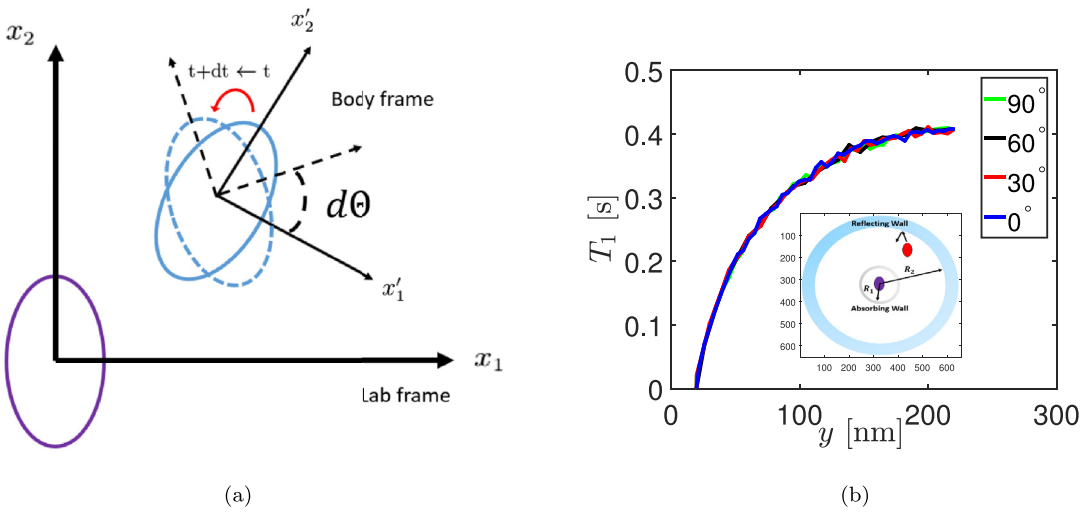

Fig. 7. (a) A cartoon of rotational motion. Initially both the moving inclusion and the centered inclusion are set to $\varphi_{\frac{\pi}{2}}$ types (i.e. $\Theta = 90^\circ$), but as time progresses the diffusing inclusion is allowed to rotate. (b) gives a prediction of the first passage time using Langevin dynamics. The inset shows a reflecting boundary condition at R_2 and an absorbing boundary condition at R_1.

Setting $I = 0$ in Eq. (43) and combining with Eq. (36), we get,

$$d\Theta = -\frac{1}{\nu_\theta}\frac{\partial \phi}{\partial \Theta}dt + \sqrt{\frac{2k_BTdt}{\nu_\theta}}\xi_\theta, \tag{45}$$

$$dr_{i'} = -\nu_{i'j'}^{-1}\frac{\partial \phi}{\partial r_{j'}}dt + \sqrt{\frac{2k_BTdt}{\nu_{i'i'}}}\xi_{i'} \text{ (no sum in the second term).} \tag{46}$$

where $\xi_\theta, \xi_{i'} \sim \mathcal{N}(0,1)$ and index i', j' refer to body frame x_1', x_2' (see Fig. 7(a)). With the center of the moving inclusion fixed at each node on the grid, we can compute the total free energy in 6 directions ($\Theta_{1,2,3,4,5,6} = 30^\circ, 90^\circ, 150^\circ, 210^\circ, 270^\circ, 330^\circ$, see Fig. 4(a)). We compute $\frac{\partial \phi}{\partial \Theta}$ in these six directions by a forward Euler method denoted as $\phi_{\Theta_1}, \phi_{\Theta_2}, \phi_{\Theta_3}, \phi_{\Theta_4}, \phi_{\Theta_5}, \phi_{\Theta_6}$, respectively. Then, for any Θ such that $\Theta_{m-1} < \Theta < \Theta_m$, we use linear interpolations of $\phi_{\Theta_{m-1}}$ and ϕ_{Θ_m} to approximate $\frac{\partial \phi}{\partial \Theta}$ in the above equation.

The simulation result is shown in Fig. 7(b) whose timescale is very similar to the one without rotational effects Fig. 6(c). However, the first passage time in this case hardly depends on the initial angle α. This is in good agreement with the results in (Han et al., 2006) where the memory of initial angle α is washed out after long time if there is no external force ($\phi = 0$). We also study the distributions of the orientation of the moving particle when it crosses the inner boundary $r = R_1$. The result is shown in Fig. 8. It seems that the moving particle crosses the inner boundary at angle around 60° and 240° with slightly higher probability, but this could be an artifact of our triangular grid. Rather, it is likely that all orientations are more or less equally probable when the particle crosses the $r = R_1$ boundary, but when the two particles coalesce they eventually adopt orientations corresponding to the minimum free energy state.

4. Hydrodynamic interactions of two circular inclusions

As a particle is moving along its trajectory, it will disturb the velocity field of the fluid around it. As a consequence, the viscous drag force exerted on other particles is also changed. This fluid-mediated hydrodynamic interaction between different particles is captured using the Oseen tensor $\boldsymbol{\Omega}(\mathbf{r_1} - \mathbf{r_2})$ which depends on the position of the particles $\mathbf{r_1}$ and $\mathbf{r_2}$. Let $\mathbf{F_1}$ be the force acting on inclusion 1 and $\mathbf{F_2}$ be the force acting on inclusion 2, then the velocity of the two inclusions are given by Doi and Edwards (1988), Öttinger (1996),

$$\mathbf{V_1} = \boldsymbol{\Omega}(\mathbf{0}) \cdot \mathbf{F_1} + \boldsymbol{\Omega}(\mathbf{r_1} - \mathbf{r_2}) \cdot \mathbf{F_2} + \sqrt{2}\ \mathbf{B}(\mathbf{r_1} - \mathbf{r_2}) \cdot \boldsymbol{\xi_1} \tag{47}$$

$$\mathbf{V_2} = \boldsymbol{\Omega}(\mathbf{r_2} - \mathbf{r_1}) \cdot \mathbf{F_1} + \boldsymbol{\Omega}(\mathbf{0}) \cdot \mathbf{F_2} + \sqrt{2}\ \mathbf{B}(\mathbf{r_1} - \mathbf{r_2}) \cdot \boldsymbol{\xi_2}, \tag{48}$$

where $[\boldsymbol{\xi_k}]_j, k \in \{0, 1, 2\}$ are random vectors with expectation values $\langle [\boldsymbol{\xi_k}]_j \rangle = 0$, $\langle [\boldsymbol{\xi_k}]_i(t), [\boldsymbol{\xi_k}]_j(t') \rangle = \delta_{ij}\delta(t - t')$, and a 2D version of the Oseen tensor $\boldsymbol{\Omega}(\mathbf{r})$ is given by Di Leonardo et al. (2008),

$$\boldsymbol{\Omega}(\mathbf{r}) = \begin{cases} \frac{1}{4\pi\eta_m}\left[\log\left(\frac{L}{r} - 1\right)\mathbf{I} + \frac{\mathbf{r}\otimes\mathbf{r}}{r^2}\right], & \mathbf{r} \neq \mathbf{0}; \\ \frac{\mathbf{I}}{\nu}, & \mathbf{r} = \mathbf{0}. \end{cases} \tag{49}$$

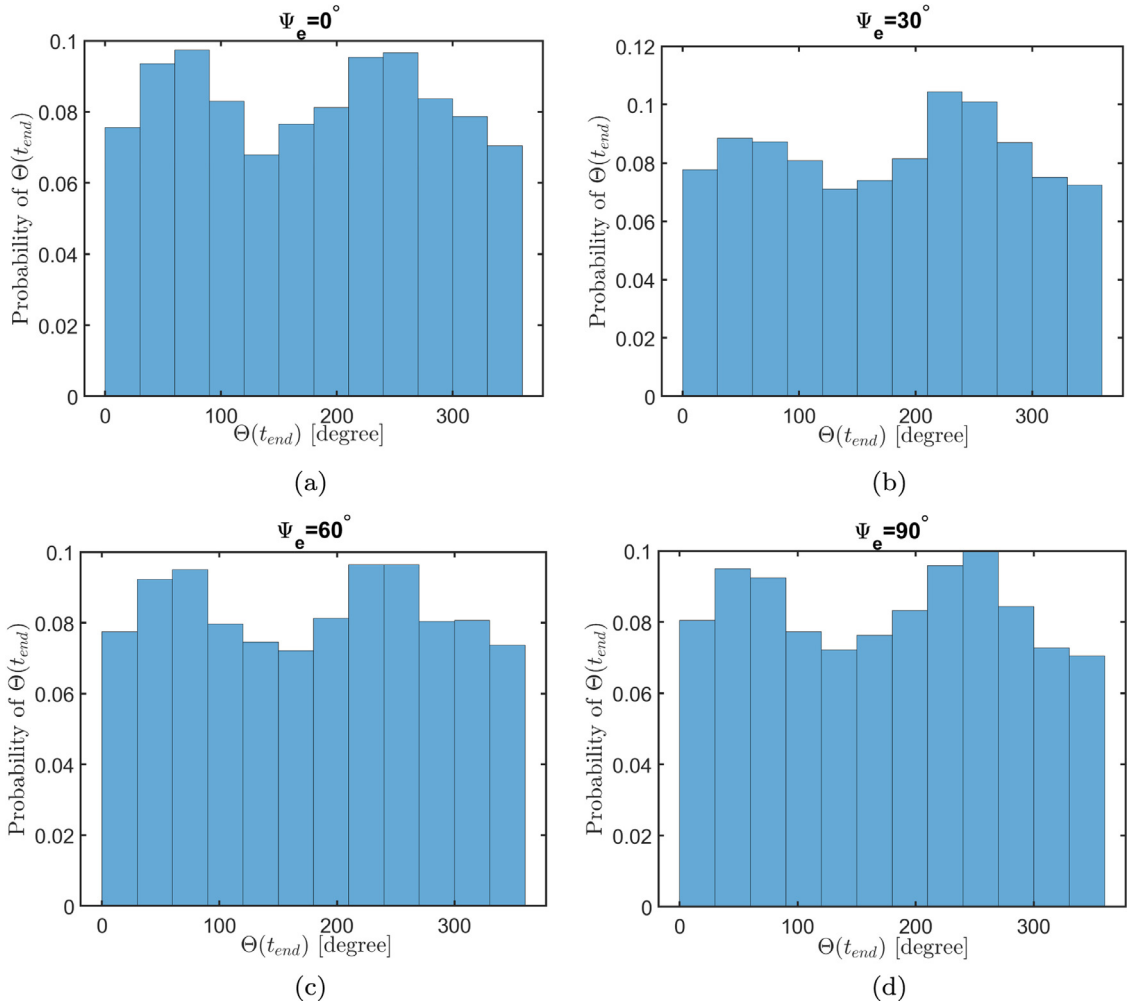

Fig. 8. The probability distributions of the orientation of the moving particle when it crosses the inner boundary R_1 under four initial orientation $\Psi_e = 0^\circ, 30^\circ, 60^\circ, 90^\circ$ and some appropriately chosen initial positions y such that the memory of the initial angle $\Theta(0)$ is washed out when the inner boundary is crossed.

In the above L is the side of the square membrane, r is the center to center distance between two inclusions. The weighting factors $\mathbf{B}$ in Eqn. (47)–(48) are the square root of the diffusion tensor $\mathbf{D}$ that is modified to include the hydrodynamic interaction,

$$\mathbf{D} = \frac{k_B T}{\nu}(\mathbf{I} + \nu\boldsymbol{\Omega}), \quad \mathbf{D}_{ij} = \mathbf{B}_{ik} \cdot \mathbf{B}^T_{jk}, \tag{50}$$

and $\mathbf{I}$ is second order identity tensor. In our model, since the inclusion 1 is always fixed, $\mathbf{V_1} = 0$. We choose the center of inclusion 1 as the origin and use $\mathbf{r} = \mathbf{r_2}$ for brevity. Then,

$$\mathbf{F_1} = -\nu\boldsymbol{\Omega}(\mathbf{r}) \cdot \mathbf{F_2} - \nu\sqrt{2}\ \mathbf{B}(\mathbf{r}) \cdot \boldsymbol{\xi_1}. \tag{51}$$

$$\Longrightarrow \mathbf{V_2} = \left(-\nu\boldsymbol{\Omega}^2(\mathbf{r}) + \frac{\mathbf{I}}{\nu}\right) \cdot \mathbf{F_2} - \nu\sqrt{2}\boldsymbol{\Omega}(\mathbf{r}) \cdot \mathbf{B}(\mathbf{r}) \cdot \boldsymbol{\xi_1} + \sqrt{2}\ \mathbf{B}(\mathbf{r}) \cdot \boldsymbol{\xi_2}. \tag{52}$$

Since the sum of two mutually independent normal random vectors is also a normal random vector, we can find a normal random vector $[\boldsymbol{\xi_0}]_j$, such that,

$$d\mathbf{r} = \mathbf{V_2}dt = \mathbf{G}(\mathbf{r}) \cdot \mathbf{F_2}dt + \sqrt{2}\ \bar{\mathbf{B}}(\mathbf{r}) \cdot \boldsymbol{\xi_0}dt, \tag{53}$$

where the effective drift tensor $\mathbf{G}$, effective diffusion tensor $\bar{\mathbf{D}}$, and effective weighting factors $\bar{\mathbf{B}}$ are given by,

$$\mathbf{G}(\mathbf{r}) = \left(-\nu\boldsymbol{\Omega}^2(\mathbf{r}) + \frac{\mathbf{I}}{\nu}\right), \quad \bar{\mathbf{D}} = \bar{\mathbf{B}}^2 = \nu^2\boldsymbol{\Omega}\mathbf{B}^2\boldsymbol{\Omega} + \mathbf{B}^2. \tag{54}$$

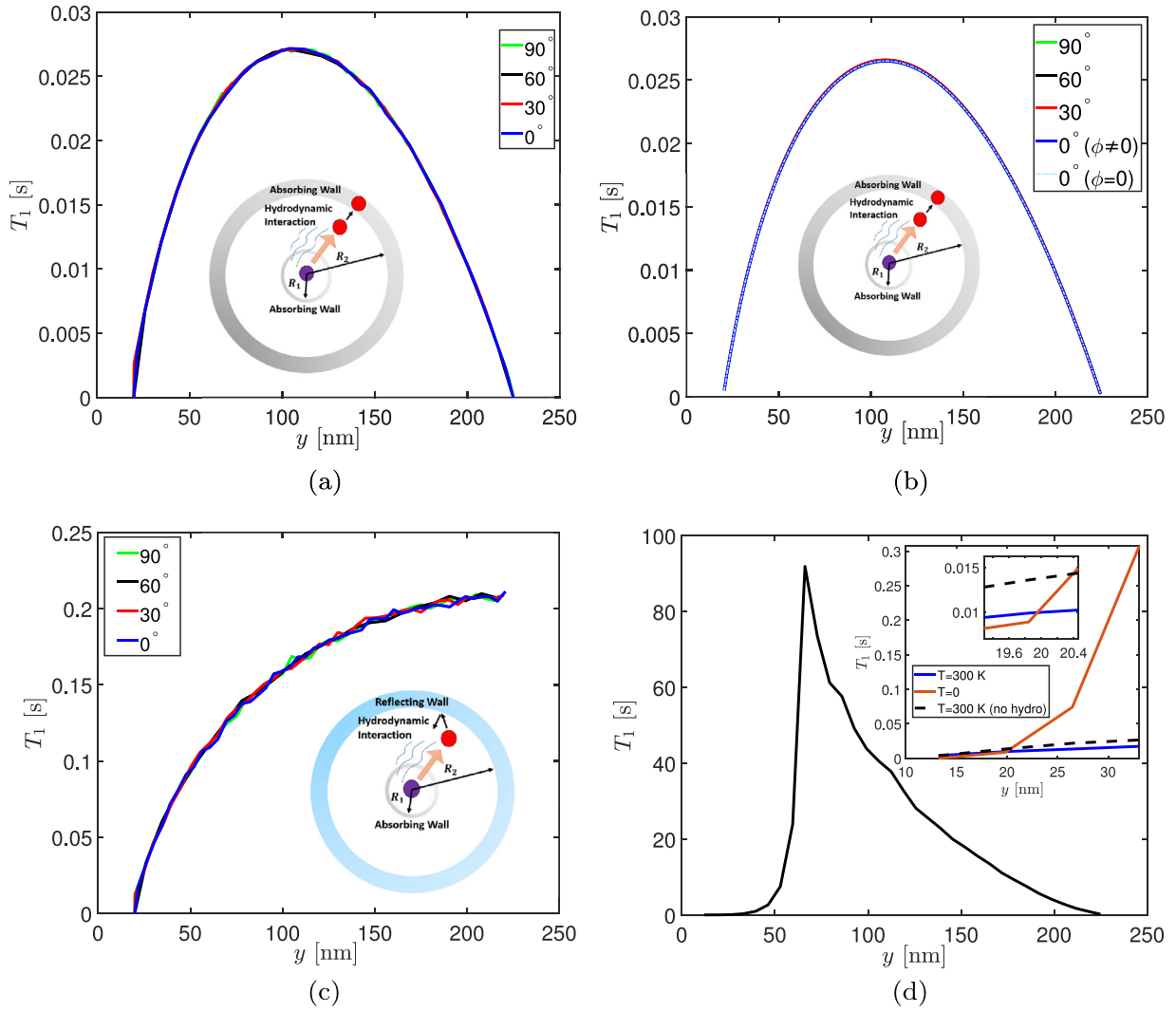

Fig. 9. The first passage time under different initial angle $\alpha = 90^\circ, 60^\circ, 30^\circ, 0^\circ$ derived from (a) Langevin dynamics and (b) Fokker-Planck equation. The insets of these two plots show two absorbing boundary conditions at R_1 and R_2. In addition, a comparison is made at $\alpha = 0^\circ$ between interaction force added ($\phi \neq 0$) and removed ($\phi = 0$). (c) gives a prediction for the first passage time using Langevin dynamics. The inset shows a reflecting boundary condition at R_2 and an absorbing boundary condition at R_1 by (d) The black curve describes the first passage time without thermal fluctuation ($T = 0$) at $\alpha = 49.1^\circ$. The inset is a comparison of the first passage time between $T = 300$ K (blue curve) and $T = 0$ (red curve) under hydrodynamic interactions and initial angle $\alpha = 49.1^\circ$. The black dashed curve implies that when $T = 300$ K hydrodynamic interactions speed up self-assembly. (For interpretation of the references to colour in this figure legend, the reader is referred to the web version of this article.)

Accordingly, the corresponding Fokker-Planck equation is a parabolic partial differential equation,

$$\begin{aligned}\frac{\partial p}{\partial t} &= \frac{\partial}{\partial x_i}\left[G_{ij}\frac{\partial \phi}{\partial x_j}p\right] + \frac{\partial^2}{\partial x_i \partial x_j}\left[\bar{D}_{ij}p\right] \\ &= -\left[-\frac{\partial}{\partial x_i}\left(\bar{D}_{ij}\frac{\partial p}{\partial x_j}\right) - \left(G_{ij}\frac{\partial \phi}{\partial x_j} + \frac{\partial \bar{D}_{ij}}{\partial x_j}\right)\frac{\partial p}{\partial x_i} - \left(\frac{\partial}{\partial x_i}\left(G_{ij}\frac{\partial \phi}{\partial x_j}\right) + \frac{\partial^2 \bar{D}_{ij}}{\partial x_i \partial x_j}\right)p\right].\end{aligned} \tag{55}$$

We transform Eq. (55) into polar coordinates (see Appendix D), to get

$$\frac{\partial p}{\partial t} = \frac{\partial^2 p}{\partial r^2}H_1(r,\theta) + \frac{\partial^2 p}{\partial \theta^2}H_2(r,\theta) + \frac{\partial^2 p}{\partial r \partial \theta}H_3(r,\theta) + \frac{\partial p}{\partial r}H_4(r,\theta) + \frac{\partial p}{\partial \theta}H_5(r,\theta) + pH_6(r,\theta). \tag{56}$$

In the above, H_1, H_2, H_3, H_4, H_5, H_6 are functions given in the Appendix. Using similar methods as before, a PDE for the first passage time can be derived (see Appendix D). We performed Langevin dynamic calculations as well as numerical integration of the PDE and the results are given in Fig. 9.

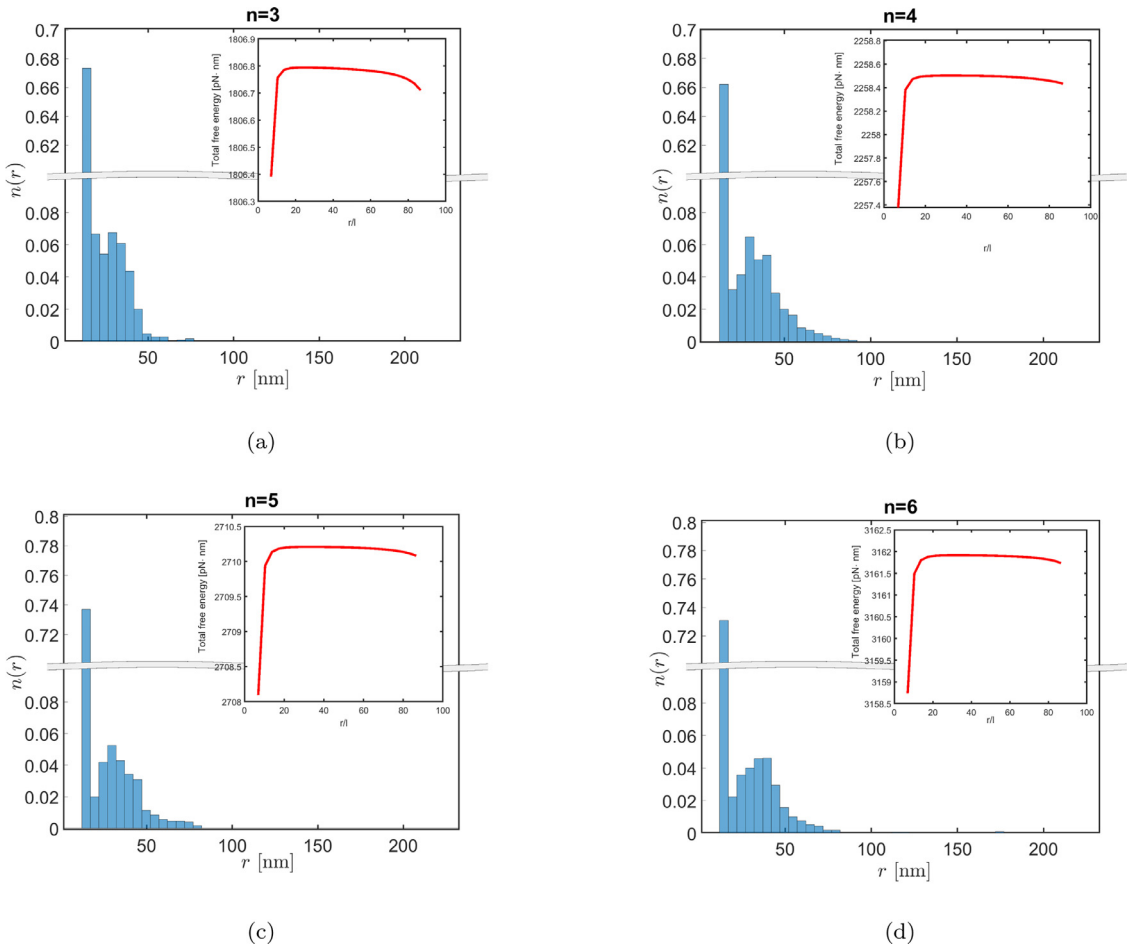

Fig. 10. The probability distributions as a function of inclusion position after 30 time steps (1.92×10^{-5} s each time step). We divide radial direction into 43 evenly-spaced intervals of width 5 nm and count the number of moving inclusions in each interval after 30 time steps. Then, we use these numbers and divide by the total number of moving inclusions in 350 runs to get $n(r)$. E.g. if $n_{\text{mov}} = 3$ and the number of particles in the left most interval is 100, then the $n(r)$ for that interval is computed by $100/(350 \times 3)$. In each figure the inset is the total free energy of the membrane inclusion system as a function of separation (all inclusions are the same distance away from the center inclusion).

The excellent agreement between Fig. 9(a) and (b) again proves the effectiveness of our methods. From these two figures we also learn that the first passage time is not sensitive to the initial angle α for circular inclusions. Fig. 9(b) shows that the Brownian motion is still dominant in the context of hydrodynamic interaction. Fig. 9(c) predicts the first passage time when the outer boundary is replaced by reflecting boundary condition. A comparison of Fig. 3(d) and Fig. 9(d) shows that hydrodynamic interactions speed up self-assembly for two circular inclusions when $T = 300$ K (in agreement with (Matthews and Likos, 2013)) and slow down self-assembly when $T = 0$. On the other hand, Rower et al. (2019) show that hydrodrodynamic effects may not always speed up self-assembly of circular particles. However, our model is different from the one in (Rower et al., 2019) since (1) we fixed one inclusion in the center while they let both inclusions diffuse, and (2) we considered a flat lipid membrane while they performed computations on a spherical surface. Nevertheless, our results and those of Rower et al. (2019) agree on the point that the coalescence time in the presence or absence of hydrodynamic interactions is of the same order of magnitude. The form of the black curve in Fig. 9(d) is similar to Fig. 3(d).

5. Self-assembly of multiple inclusions

In this section, we use Langevin dynamics to study the self-assembly of multiple inclusions. The inset of Fig. 3(d) shows that self-assembly can be finished quickly at small separations where the interaction force is dominant. To verify this idea we study the self-assembly of three to six moving inclusions which are initially 16 nm away from the fixed inclusion at the center. In order to quantify the self-assembly of multiple inclusions, we compute probability distribution $n(r)$ (of finding an inclusion between r and $r + dr$) after 30 time steps and compare between number of moving inclusions ($n_{\text{mov}} = 3, 4, 5, 6$). Due to limitations of computational power, we do not consider hydrodynamic interactions and run simulations 350 times for each case. Fig. 10 shows that inclusions are slightly more likely to be absorbed to the center with a large number of moving

inclusions ($n_{\text{mov}} = 5, 6$) than with small number. ($n_{\text{mov}} = 3, 4$). It seems that at small initial separations self-assembly could be finished sooner with more moving inclusions due to a stronger interaction force.

Our results in this section are limited by a lack of computational power. The calculation of the force on each inclusion in a cluster at every time-step is expensive since the equilibrium configuration of the membrane must be computed repeatedly and then numerical differentiation of the free energy of the whole system must be carried out. We were able to speed up this computation for two inclusions by tabulating the free energy of the membrane-inclusion system for every nodal position of the moving inclusion (remember that one of the inclusions is fixed at the center). This method is not practical if there are multiple moving inclusions, so we must resort to other techniques which we leave for future work.

6. Conclusions

In this paper we have analyzed the self-assembly of inclusions on a lipid membrane under the influence of elastic and entropic interaction forces that have their origin in the bending deformation of the membrane. We have shown that the self-assembly process is dominated by diffusion, but the attractive interaction forces come into play at small separations. Unlike most earlier works that use various simulation techniques (such as Monte Carlo, molecular dynamics and various coarse-grained methods that account for Brownian motion), we use both Langevin dynamics and the corresponding Fokker-Planck equation to cast the self-assembly as a first passage time problem. We show that these two methods are in excellent agreement for circular and elliptical inclusions and in the presence of hydrodynamic interactions. Our ideas provide a different view of self-assembly that is based on partial differential equations (for the first passage time) that could be leveraged for creating fast computational methods. One such class of methods is based on fluctuating hydrodynamics (Donev et al., 2010) which extend computatioanl techniques for fluid-structure interactions to problems with Brownian motion. Although we only demonstrate our techniques here using interaction forces based on membrane curvature, we can extend them to account for membrane thickness mediated and other (e.g., electrostatic) interactions.

Declaration of Competing Interest

None.

Acknowledgement

We acknowledge support for this work from a National Science Foundation grant NSF CMMI 1662101.

Appendix A. Computing the ODE for the first passage time for circular inclusions

Integrate Eq. (20) for P over all $t \geq 0$,

$$\int_0^\infty \frac{\partial P}{\partial t} dt = \frac{\partial}{\partial r}\left[\frac{1}{\nu}\frac{\partial \phi}{\partial r} g_1 + D\frac{\partial g_1}{\partial r}\right] + \frac{1}{r}\left[\frac{1}{\nu}\frac{\partial \phi}{\partial r} g_1 + D\frac{\partial g_1}{\partial r}\right] \tag{A.1}$$

$$-\frac{1}{r}\delta(r-y) = \mathcal{L}_r g_1(r,y), \tag{A.2}$$

where $\frac{1}{r}\delta(r-y)$ is the initial condition and the second order linear differential operator $\mathcal{L}_r : \mathcal{D}(\mathcal{L}_r) \subset H_0^1([R_1, R_2]) \to H_0^1([R_1, R_2])$ is defined as,

$$\mathcal{L}_r = \frac{\partial}{\partial r}\left[\frac{1}{\nu}\frac{\partial \phi}{\partial r} + D\frac{\partial}{\partial r}\right] + \frac{1}{r}\left[\frac{1}{\nu}\frac{\partial \phi}{\partial r} + D\frac{\partial}{\partial r}\right], \tag{A.3}$$

with domain

$$\mathcal{D}(\mathcal{L}_r) = \left\{u \in H_0^1([R_1, R_2]) | u(R_1) = u(R_2) = 0\right\}, \tag{A.4}$$

and the inner product is defined as,

$$\langle u, v\rangle = \int_{R_1}^{R_2} uv dr, \quad \forall u, v \in \mathcal{D}(\mathcal{L}_r). \tag{A.5}$$

It is useful to obtain the adjoint operator $\mathcal{L}_r^*$ (see Appendix D for the detailed procedure to derive the adjoint operator) which satisfies $\langle v, \mathcal{L}_r u\rangle = \langle \mathcal{L}_r^* v, u\rangle, \ \forall u, v \in \mathcal{D}(\mathcal{L}_r)$,

$$\mathcal{L}_r^* = -\frac{1}{\nu}\frac{\partial \phi}{\partial r}\frac{\partial}{\partial r} + D\frac{\partial^2}{\partial r^2} + \frac{1}{\nu}\frac{\partial \phi}{\partial r}\frac{1}{r} - D\frac{\partial \frac{1}{r}}{\partial r}. \tag{A.6}$$

Note that $\mathcal{L}_r$ and $\mathcal{L}_r^*$ are uniformly elliptic, then $\mathcal{L}_r^{-1}$ and $\mathcal{L}_r^{*-1}$ exist (Evans, 2010). It immediately follows from Eq. (A.2) that,

$$g_1 = -\mathcal{L}_r{}^{-1}\frac{1}{r}\delta(r-y). \tag{A.7}$$

Put Eq. (A.7) into Eq. (24) and use the fact that ${\mathcal{L}_r}^{-1^*} = {\mathcal{L}_r}^{*-1}$, then,

$$T_1(y) = -\int_{R_1}^{R_2} r{\mathcal{L}_r}^{-1}\frac{1}{r}\delta(r-y)dr \tag{A.8}$$

$$= -\int_{R_1}^{R_2} \frac{1}{r}\delta(r-y){\mathcal{L}_r}^{*-1}rdr \tag{A.9}$$

$$= -\frac{1}{y}{\mathcal{L}_y}^{*-1}y \tag{A.10}$$

$$\Longrightarrow \mathcal{L}_y^* y T_1(y) = -y. \tag{A.11}$$

Using Eq. (A.6), we can derive a second order ODE for $T_1(y)$ Eq. (26).

Appendix B. Computing the PDE for the first passage time for elliptical inclusions

Transforming to polar coordinates, Eq. (37) reads,

$$\begin{aligned}
\frac{\partial p}{\partial t} &= \frac{1}{\nu_a}\Bigg[p\cos^2\theta\frac{\partial^2\phi}{\partial r^2} + p\frac{\partial\phi}{\partial r}\frac{\sin^2\theta}{r} - p\frac{\sin 2\theta}{r}\frac{\partial^2\phi}{\partial r\partial\theta} + p\frac{\sin 2\theta}{r^2}\frac{\partial\phi}{\partial\theta} + p\frac{\sin^2\theta}{r^2}\frac{\partial^2\phi}{\partial\theta^2} \\
&\quad + \left(\cos\theta\frac{\partial\phi}{\partial r} - \frac{\sin\theta}{r}\frac{\partial\phi}{\partial\theta}\right)\left(\cos\theta\frac{\partial p}{\partial r} - \frac{\sin\theta}{r}\frac{\partial p}{\partial\theta}\right)\Bigg] \\
&\quad + \frac{1}{\nu_b}\Bigg[p\sin^2\theta\frac{\partial^2\phi}{\partial r^2} + p\frac{\partial\phi}{\partial r}\frac{\cos^2\theta}{r} + p\frac{\sin 2\theta}{r}\frac{\partial^2\phi}{\partial r\partial\theta} - p\frac{\sin 2\theta}{r^2}\frac{\partial\phi}{\partial\theta} + p\frac{\cos^2\theta}{r^2}\frac{\partial^2\phi}{\partial\theta^2} \\
&\quad + \left(\sin\theta\frac{\partial\phi}{\partial r} + \frac{\cos\theta}{r}\frac{\partial\phi}{\partial\theta}\right)\left(\sin\theta\frac{\partial p}{\partial r} + \frac{\cos\theta}{r}\frac{\partial p}{\partial\theta}\right)\Bigg] \\
&\quad + D_a\left[\cos^2\theta\frac{\partial^2 p}{\partial r^2} + \frac{\sin^2\theta}{r}\frac{\partial p}{\partial r} - \frac{\sin 2\theta}{r}\frac{\partial^2 p}{\partial r\partial\theta} + \frac{\sin 2\theta}{r^2}\frac{\partial p}{\partial\theta} + \frac{\sin^2\theta}{r^2}\frac{\partial^2 p}{\partial\theta^2}\right] \\
&\quad + D_b\left[\sin^2\theta\frac{\partial^2 p}{\partial r^2} + \frac{\cos^2\theta}{r}\frac{\partial p}{\partial r} + \frac{\sin 2\theta}{r}\frac{\partial^2 p}{\partial r\partial\theta} - \frac{\sin 2\theta}{r^2}\frac{\partial p}{\partial\theta} + \frac{\cos^2\theta}{r^2}\frac{\partial^2 p}{\partial\theta^2}\right]
\end{aligned} \tag{B.1}$$

$$= \mathcal{F}_{r,\theta}p, \tag{B.2}$$

where the elliptic differential operator $\mathcal{F}_{r,\theta} : \mathcal{D}(\mathcal{F}_{r,\theta}) \subset H_0^1([R_1,R_2]\times[0,2\pi]) \to H_0^1([R_1,R_2]\times[0,2\pi])$ is in divergence form, with domain

$$\mathcal{D}(\mathcal{F}_{r,\theta}) = \left\{u \in H_0^1([R_1,R_2]\times[0,2\pi]) | u(R_1,\theta) = u(R_2,\theta) = 0,\ u(r,0) = u(r,2\pi)\right\}, \tag{B.3}$$

and the inner product is defined as,

$$\langle u, v\rangle = \int_{R_1}^{R_2}\int_0^{2\pi} uv dr d\theta, \quad \forall u, v \in \mathcal{D}(\mathcal{F}_{r,\theta}). \tag{B.4}$$

Then, we can derive $\mathcal{F}_{r,\theta}^*$, the adjoint operator of $\mathcal{F}_{r,\theta}$, satisfying $\langle v, \mathcal{F}_{r,\theta}u\rangle = \langle \mathcal{F}_{r,\theta}^* v, u\rangle$, $\forall u, v \in \mathcal{D}(\mathcal{F}_{r,\theta})$,

$$\begin{aligned}
\mathcal{F}_{r,\theta}^* &= \frac{1}{\nu_a}\left[\frac{\cos^2\theta}{r}\frac{\partial\phi}{\partial r} - \frac{\sin 2\theta}{2r^2}\frac{\partial\phi}{\partial\theta} - \left(\cos^2\theta\frac{\partial\phi}{\partial r} - \frac{\sin 2\theta}{2r}\frac{\partial\phi}{\partial\theta}\right)\frac{\partial}{\partial r} + \left(\frac{\sin 2\theta}{2r}\frac{\partial\phi}{\partial r} - \frac{\sin^2\theta}{r^2}\frac{\partial\phi}{\partial\theta}\right)\frac{\partial}{\partial\theta}\right] \\
&\quad + \frac{1}{\nu_b}\left[\frac{\sin^2\theta}{r}\frac{\partial\phi}{\partial r} + \frac{\sin 2\theta}{2r^2}\frac{\partial\phi}{\partial\theta} - \left(\sin^2\theta\frac{\partial\phi}{\partial r} + \frac{\sin 2\theta}{2r}\frac{\partial\phi}{\partial\theta}\right)\frac{\partial}{\partial r} - \left(\frac{\sin 2\theta}{2r}\frac{\partial\phi}{\partial r} + \frac{\cos^2\theta}{r^2}\frac{\partial\phi}{\partial\theta}\right)\frac{\partial}{\partial\theta}\right] \\
&\quad + D_a\Bigg[\cos^2\theta\frac{\partial^2}{\partial r^2} + \frac{\sin^2\theta}{r^2}\frac{\partial^2}{\partial\theta^2} - \frac{\sin 2\theta}{r}\frac{\partial^2}{\partial r\partial\theta} - \left(\frac{\sin^2\theta + 2\cos 2\theta}{r}\right)\frac{\partial}{\partial r} + \frac{2\sin 2\theta}{r^2}\frac{\partial}{\partial\theta} \\
&\quad + \frac{\sin^2\theta + 2\cos 2\theta}{r^2}\Bigg] \\
&\quad + D_b\Bigg[\sin^2\theta\frac{\partial^2}{\partial r^2} + \frac{\cos^2\theta}{r^2}\frac{\partial^2}{\partial\theta^2} + \frac{\sin 2\theta}{r}\frac{\partial^2}{\partial r\partial\theta} - \left(\frac{\cos^2\theta - 2\cos 2\theta}{r}\right)\frac{\partial}{\partial r} - \frac{2\sin 2\theta}{r^2}\frac{\partial}{\partial\theta} \\
&\quad + \frac{\cos^2\theta - 2\cos 2\theta}{r^2}\Bigg].
\end{aligned} \tag{B.5}$$

After q_1 is defined in Eq. (40), we integrate Eq. (B.2) for p over all $t \geq 0$,

$$\int_0^\infty \frac{\partial p}{\partial t} dt = \frac{\partial}{\partial r}\left[\frac{1}{\nu}\frac{\partial \phi}{\partial r} q_1 + D\frac{\partial q_1}{\partial r}\right] + \frac{1}{r}\left[\frac{1}{\nu}\frac{\partial \phi}{\partial r} q_1 + D\frac{\partial q_1}{\partial r}\right] + \frac{1}{r}\frac{\partial}{\partial \theta}\left[\frac{1}{r}\frac{q_1}{\nu}\frac{\partial \phi}{\partial \theta} + \frac{D}{r}\frac{\partial q_1}{\partial \theta}\right] \tag{B.6}$$

$$-\frac{1}{r}\delta(r-y)\delta(\theta-\alpha) = \mathcal{F}_{r,\theta} q_1, \tag{B.7}$$

Since $\mathcal{F}_{r,\theta}$ and $\mathcal{F}^*_{r,\theta}$ are uniformly elliptic, $\mathcal{F}^{-1}_{r,\theta}$ and ${\mathcal{F}^*_{r,\theta}}^{-1}$ exist (Evans, 2010). Then, it immediately follows from Eq. (B.7) that,

$$q_1 = -{\mathcal{F}_{r,\theta}}^{-1}\frac{1}{r}\delta(r-y)\delta(\theta-\alpha). \tag{B.8}$$

Put Eq. (B.8) into Eq. (39) and use the fact that $\mathcal{F}^{-1^*}_{r,\theta} = {\mathcal{F}^*_{r,\theta}}^{-1}$. We can derive,

$$T_1(y,\alpha) = -\int_{R_1}^{R_2}\int_0^{2\pi} {\mathcal{F}_{r,\theta}}^{-1}\frac{1}{r}\delta(r-y)\delta(\theta-\alpha) r d\theta dr \tag{B.9}$$

$$= -\int_{R_1}^{R_2}\int_0^{2\pi} \frac{1}{r}\delta(r-y)\delta(\theta-\alpha){\mathcal{F}^*_{r,\theta}}^{-1} r dr d\theta \tag{B.10}$$

$$= -\frac{1}{y}{\mathcal{F}^*_{y,\alpha}}^{-1} y. \tag{B.11}$$

$$\Longrightarrow \mathcal{F}^*_{y,\alpha} y T_1(y,\alpha) = -y. \tag{B.12}$$

Using Eq. (B.5), we can derive a second order PDE for $T_1(y)$ Eq. (41).

Appendix C. Finite difference method

From Kwiecinski et al. (2019), the free energy function in Eq. (41) is given by,

$$\phi(y,\alpha) = \frac{2c_1}{y^2}\cos 2\alpha + \frac{c_2}{y^4} + \frac{c_3}{y^6} + c_4. \tag{C.1}$$

Then,

$$\frac{\partial \phi}{\partial \alpha} = \frac{-4c_1}{y^2}\sin 2\alpha, \quad \frac{\partial \phi}{\partial y} = \frac{-4c_1}{y^3}\cos 2\alpha - \frac{4c_2}{y^5} - \frac{6c_3}{y^7}. \tag{C.2}$$

Let i denote the index in α direction and j in y direction. The finite difference scheme of Eq. (41) then is:

$$\kappa_1(i,j)\frac{T_{i,j+1} - 2T_{i,j} + T_{i,j-1}}{h_y^2} + \kappa_2(i,j)\frac{T_{i+1,j} - 2T_{i,j} + T_{i-1,j}}{h_\alpha^2} + \kappa_4(i,j)\frac{T_{i,j+1} - T_{i,j}}{h_y}$$
$$+ \kappa_3(i,j)\frac{T_{i+1,j+1} - T_{i+1,j-1} - T_{i-1,j+1} + T_{i-1,j-1}}{4h_\alpha h_y} + \kappa_5(i,j)\frac{T_{i+1,j} - T_{i,j}}{h_\alpha} = -1, \tag{C.3}$$

for all inner points (i, j) (see Fig. C.11) where κ_1, κ_2, κ_3, κ_4, κ_5 are given by,

$$\kappa_1(i,j) = D_a\cos^2\alpha_i + D_b\sin^2\alpha_i \tag{C.4}$$

$$\kappa_2(i,j) = D_a\frac{\sin^2\alpha_i}{y_j^2} + D_b\frac{\cos^2\alpha_i}{y_j^2} \tag{C.5}$$

$$\kappa_3(i,j) = -D_a\frac{\sin 2\alpha_i}{y_j} + D_b\frac{\sin 2\alpha_i}{y_j} \tag{C.6}$$

$$\kappa_4(i,j) = D_a\frac{\sin^2\alpha_i}{y_j} + D_b\frac{\cos^2\alpha_i}{y_j} + \frac{1}{\nu_a}\left[\frac{-4c_1\sin^2 2\alpha_i}{2y_j^3} + \cos^2\alpha_i\left(\frac{4c_1}{y_j^3}\cos 2\alpha_i + \frac{4c_2}{y_j^5} + \frac{6c_3}{y_j^7}\right)\right]$$
$$+ \frac{1}{\nu_b}\left[\frac{4c_1\sin^2 2\alpha_i}{2y_j^3} + \sin^2\alpha_i\left(\frac{4c_1}{y_j^3}\cos 2\alpha_i + \frac{4c_2}{y_j^5} + \frac{6c_3}{y_j^7}\right)\right] \tag{C.7}$$

$$\kappa_5(i,j) = D_a\frac{\sin 2\alpha_i}{y_j^2} - D_b\frac{\sin 2\alpha_i}{y_j^2} + \frac{1}{\nu_a}\left[-\frac{\sin 2\alpha_i}{2y_j}\left(\frac{4c_1}{y_j^3}\cos 2\alpha_i + \frac{4c_2}{y_j^5} + \frac{6c_3}{y_j^7}\right) + \frac{4c_1\sin 2\alpha_i\sin^2\alpha_i}{y_j^4}\right]$$
$$+ \frac{1}{\nu_b}\left[\frac{\sin 2\alpha_i}{2y_j}\left(\frac{4c_1}{y_j^3}\cos 2\alpha_i + \frac{4c_2}{y_j^5} + \frac{6c_3}{y_j^7}\right) + \frac{4c_1\sin 2\alpha_i\cos^2\alpha_i}{y_j^4}\right]. \tag{C.8}$$

The boundary conditions can be easily implemented using the fact that $T_1(R_1,\alpha) = T_1(R_2,\alpha) = 0$ and $T_1(y,0) = T_1(y,2\pi)$.

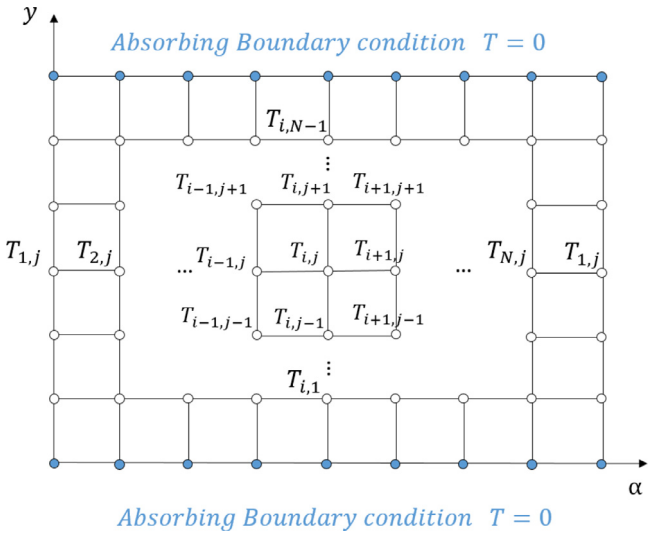

Fig. C1. Finite difference method to solve Eq. (C.3).

Appendix D. Computing the PDE for the first passage time under hydro-dynamic interaction

$$
\begin{aligned}
\frac{\partial p}{\partial t} = {} & \frac{\partial^2 p}{\partial r^2}\left[\bar{D}_{11}\cos^2\theta + \bar{D}_{22}\sin^2\theta + \bar{D}_{12}\sin 2\theta\right] \\
& + \frac{\partial^2 p}{\partial \theta^2}\left[\frac{\bar{D}_{22}\cos^2\theta + \sin\theta(\bar{D}_{11}\sin\theta - 2\cos\theta\bar{D}_{12})}{r^2}\right] \\
& + \frac{\partial^2 p}{\partial r\partial\theta}\left[\frac{2\cos 2\theta\bar{D}_{12} + (\bar{D}_{22} - \bar{D}_{11})\sin 2\theta}{r}\right] \\
& + \frac{\partial p}{\partial r}\left[\bar{D}_{22}\cos^2\theta + 2\frac{\partial \bar{D}_{12}}{\partial\theta}\cos^2\theta + 2r\frac{\partial \bar{D}_{11}}{\partial r}\cos^2\theta + rg_{11}\frac{\partial\phi}{\partial r}\cos^2\theta - 2\bar{D}_{12}\sin\theta\cos\theta\right. \\
& - 2\sin\theta\frac{\partial \bar{D}_{11}}{\partial\theta}\cos\theta + 4r\sin\theta\frac{\partial \bar{D}_{12}}{\partial r}\cos\theta + 2rg_{12}\sin\theta\frac{\partial\phi}{\partial r}\cos\theta + \bar{D}_{11}\sin^2\theta - 2\sin^2\theta\frac{\partial \bar{D}_{12}}{\partial\theta} \\
& \left. + \sin 2\theta\frac{\partial \bar{D}_{22}}{\partial\theta} + 2r\sin^2\theta\frac{\partial \bar{D}_{22}}{\partial r} + rg_{22}\sin^2\theta\frac{\partial\phi}{\partial r}\right]\cdot\frac{1}{r} \\
& + \frac{\partial p}{\partial\theta}\left[2\frac{\partial \bar{D}_{22}}{\partial\theta}\cos^2\theta + 2r\frac{\partial \bar{D}_{12}}{\partial r}\cos^2\theta - 2\bar{D}_{22}\sin\theta\cos\theta - 4\sin\theta\frac{\partial \bar{D}_{12}}{\partial\theta}\cos\theta\right. \\
& - 2r\sin\theta\frac{\partial \bar{D}_{11}}{\partial r}\cos\theta - rg_{11}\sin\theta\frac{\partial\phi}{\partial r}\cos\theta + rg_{22}\sin\theta\frac{\partial\phi}{\partial r}\cos\theta - 2\cos 2\theta\bar{D}_{12} \\
& \left. + \bar{D}_{11}\sin 2\theta + 2\sin^2\theta\frac{\partial \bar{D}_{11}}{\partial\theta} - 2r\sin^2\theta\frac{\partial \bar{D}_{12}}{\partial r} + r\sin 2\theta\frac{\partial \bar{D}_{22}}{\partial r} + rg_{12}\cos 2\theta\frac{\partial\phi}{\partial r}\right]\cdot\frac{1}{r^2} \\
& + p\left[\frac{\partial^2 \bar{D}_{22}}{\partial\theta^2}\cos^2\theta + r\frac{\partial \bar{D}_{22}}{\partial r}\cos^2\theta + r^2\frac{\partial^2 \bar{D}_{11}}{\partial r^2}\cos^2\theta - 2\sin\theta\frac{\partial \bar{D}_{22}}{\partial\theta}\cos\theta\right. \\
& - 2\sin\theta\frac{\partial^2 \bar{D}_{12}}{\partial\theta^2}\cos\theta - 2r\sin\theta\frac{\partial^2 \bar{D}_{11}}{\partial r\partial\theta}\cos\theta + \sin 2\theta\frac{\partial \bar{D}_{11}}{\partial\theta} - 2\cos 2\theta\frac{\partial \bar{D}_{12}}{\partial\theta} + \sin^2\theta\frac{\partial^2 \bar{D}_{11}}{\partial\theta^2} \\
& + r\sin^2\theta\frac{\partial \bar{D}_{11}}{\partial r} - \left(\sin\theta\frac{\partial g_{11}}{\partial\theta}(r,\theta) - r\cos\theta\frac{\partial g_{11}}{\partial r}(r,\theta)\right)\cdot r\cos\theta\frac{\partial\phi}{\partial r} \\
& + \left(\cos\theta\frac{\partial g_{12}}{\partial\theta} + r\sin\theta\frac{\partial g_{12}}{\partial r}\right)\cdot r\cos\theta\frac{\partial\phi}{\partial r} - \left(\sin\theta\frac{\partial g_{12}}{\partial\theta} - r\cos\theta\frac{\partial g_{12}}{\partial r}\right)\cdot r\sin\theta\frac{\partial\phi}{\partial r} \\
& \left. + \left(\cos\theta\frac{\partial g_{22}}{\partial\theta} + r\sin\theta\frac{\partial g_{22}}{\partial r}(r,\theta)\right)\cdot r\sin\theta\frac{\partial\phi}{\partial r} + r\sin 2\theta\frac{\partial^2 \bar{D}_{22}}{\partial r\partial\theta}\right.
\end{aligned}
$$

$$+r\left(-\sin 2\theta\frac{\partial \bar{D}_{12}}{\partial r}+2\cos 2\theta\frac{\partial^2 \bar{D}_{12}}{\partial r\partial\theta}+r\sin 2\theta\frac{\partial^2 \bar{D}_{12}}{\partial r^2}\right)+r^2\sin^2\theta\frac{\partial^2 \bar{D}_{22}}{\partial r^2}$$
$$+g_{11}r\left(r\frac{\partial^2\phi}{\partial r^2}\cos^2\theta+\sin^2\theta\frac{\partial\phi}{\partial r}\right)+2g_{12}r\left(-\cos\theta\sin\theta\frac{\partial\phi}{\partial r}+r\cos\theta\sin\theta\frac{\partial^2\phi}{\partial r^2}\right)$$
$$+g_{22}r\left(\frac{\partial\phi}{\partial r}\cos^2\theta+r\sin^2\theta\frac{\partial^2\phi}{\partial r^2}\right)\Bigg]\cdot\frac{1}{r^2} \tag{D.1}$$

$$\triangleq \frac{\partial^2 p}{\partial r^2}H_1(r,\theta)+\frac{\partial^2 p}{\partial\theta^2}H_2(r,\theta)+\frac{\partial^2 p}{\partial r\partial\theta}H_3(r,\theta)+\frac{\partial p}{\partial r}H_4(r,\theta)+\frac{\partial p}{\partial\theta}H_5(r,\theta)$$
$$+pH_6(r,\theta) \tag{D.2}$$

$$=\mathcal{H}_{r,\theta}p, \tag{D.3}$$

where the second order linear differential operator $\mathcal{H}_{r,\theta}:\mathcal{D}(\mathcal{H}_{r,\theta})\subset H_0^1([R_1,R_2]\times[0,2\pi])\to H_0^1([R_1,R_2]\times[0,2\pi])$ is defined as,

$$\mathcal{H}_{r,\theta}=H_1(r,\theta)\frac{\partial^2}{\partial r^2}+H_2(r,\theta)\frac{\partial^2}{\partial\theta^2}+H_3(r,\theta)\frac{\partial^2}{\partial r\partial\theta}+H_4(r,\theta)\frac{\partial}{\partial r}+H_5(r,\theta)\frac{\partial}{\partial\theta}+H_6(r,\theta), \tag{D.4}$$

with domain

$$\mathcal{D}(\mathcal{H}_{r,\theta})=\left\{u\in H_0^1([R_1,R_2]\times[0,2\pi])|u(R_1,\theta)=u(R_2,\theta)=0,\ u(r,0)=u(r,2\pi)\right\}. \tag{D.5}$$

It can be shown that there exists a positive lower bound on the minimum eigenvalues of $\bar{D}$, then $\mathcal{H}_{r,\theta}$ is uniformly elliptic. To solve the adjoint operator $\mathcal{H}^*_{r,\theta}$, we just start from the definition $\forall u,v\in\mathcal{D}$,

$$\int_0^{2\pi}\int_{R_1}^{R_2}v\mathcal{H}_{r,\theta}u dr d\theta=\int_0^{2\pi}\int_{R_1}^{R_2}v\frac{\partial^2 u}{\partial r^2}H_1(r,\theta)+v\frac{\partial^2 u}{\partial\theta^2}H_2(r,\theta)+v\frac{\partial^2 u}{\partial r\partial\theta}H_3(r,\theta)+v\frac{\partial u}{\partial r}H_4(r,\theta)$$
$$+v\frac{\partial u}{\partial\theta}H_5(r,\theta)+vH_6(r,\theta)u dr d\theta \tag{D.6}$$

$$=\int_0^{2\pi}\int_{R_1}^{R_2}-\frac{\partial u}{\partial r}\frac{\partial vH_1(r,\theta)}{\partial r}-\frac{\partial u}{\partial\theta}\frac{\partial vH_2(r,\theta)}{\partial\theta}-\frac{\partial u}{\partial r}\frac{\partial vH_3(r,\theta)}{\partial\theta}-u\frac{\partial vH_4}{\partial r}$$
$$-u\frac{\partial vH_5(r,\theta)}{\partial\theta}+vH_6(r,\theta)u dr d\theta \tag{D.7}$$

$$=\int_0^{2\pi}\int_{R_1}^{R_2}u\frac{\partial^2 vH_1(r,\theta)}{\partial r^2}+u\frac{\partial^2 vH_2(r,\theta)}{\partial\theta^2}+u\frac{\partial^2 vH_3(r,\theta)}{\partial\theta\partial r}-u\frac{\partial vH_4}{\partial r}$$
$$-u\frac{\partial vH_5(r,\theta)}{\partial\theta}+uH_6(r,\theta)v dr d\theta \tag{D.8}$$

$$=\int_0^{2\pi}\int_{R_1}^{R_2}u\left[\frac{\partial^2 v}{\partial r^2}H_1+2\frac{\partial v}{\partial r}\frac{\partial H_1}{\partial r}+v\frac{\partial^2 H_1}{\partial r^2}\right]+u\left[\frac{\partial^2 v}{\partial\theta^2}H_2+2\frac{\partial v}{\partial\theta}\frac{\partial H_2}{\partial\theta}+v\frac{\partial^2 H_2}{\partial\theta^2}\right]$$
$$+u\left[\frac{\partial^2 v}{\partial\theta\partial r}H_3+\frac{\partial v}{\partial\theta}\frac{\partial H_3}{\partial r}+\frac{\partial v}{\partial r}\frac{\partial H_3}{\partial\theta}+\frac{\partial^2 H_3}{\partial\theta\partial r}v\right]-u\left[v\frac{\partial H_4}{\partial r}+H_4\frac{\partial v}{\partial r}\right]$$
$$-u\left[v\frac{\partial H_5}{\partial\theta}+H_5\frac{\partial v}{\partial\theta}\right]+uH_6v dr d\theta \tag{D.9}$$

$$=\int_0^{2\pi}\int_{R_1}^{R_2}u\mathcal{H}^*_{r,\theta}v dr d\theta, \tag{D.10}$$

where we have used the fact that u, v, H_1, H_2, H_3, H_4, H_5, H_6 are periodic functions with period 2π and $u(R_1,\theta)=u(R_2,\theta)=0, v(R_1,\theta)=v(R_2,\theta)=0$ when we do the integration by part. Then, it's clear to see that,

$$\mathcal{H}^*_{r,\theta}=\frac{\partial^2}{\partial r^2}H_1+2\frac{\partial}{\partial r}\frac{\partial H_1}{\partial r}+\frac{\partial^2 H_1}{\partial r^2}+\frac{\partial^2}{\partial\theta^2}H_2+2\frac{\partial}{\partial\theta}\frac{\partial H_2}{\partial\theta}+\frac{\partial^2 H_2}{\partial\theta^2}+\frac{\partial^2}{\partial\theta\partial r}H_3+\frac{\partial}{\partial\theta}\frac{\partial H_3}{\partial r} \tag{D.11}$$

$$+\frac{\partial}{\partial r}\frac{\partial H_3}{\partial\theta}+\frac{\partial^2 H_3}{\partial\theta\partial r}-\frac{\partial H_4}{\partial r}-H_4\frac{\partial}{\partial r}-\frac{\partial H_5}{\partial\theta}-H_5\frac{\partial}{\partial\theta}+H_6. \tag{D.12}$$

Then, using Eq. (B.12) again for $\mathcal{H}^*_{y,\alpha}$,

$$\mathcal{H}^*_{y,\alpha} y T_1(y,\alpha) = -y, \tag{D.13}$$

from which the first passage time ODE reads,

$$H_1 \frac{\partial^2 T_1}{\partial y^2} + H_2 \frac{\partial^2 T_1}{\partial \alpha^2} + H_3 \frac{\partial^2 T_1}{\partial y \partial \alpha} + \left[\frac{2H_1}{y} + 2\frac{\partial H_1}{\partial y} + \frac{\partial H_3}{\partial \alpha} - H_4 \right] \frac{\partial T_1}{\partial y} + \left[2\frac{\partial H_2}{\partial \alpha} + \frac{\partial H_3}{\partial y} + \frac{H_3}{y} - H_5 \right] \frac{\partial T_1}{\partial \alpha}$$
$$+ \left[\frac{2}{y}\frac{\partial H_1}{\partial y} + \frac{\partial^2 H_1}{\partial y^2} + \frac{\partial^2 H_2}{\partial \alpha^2} + \frac{\partial^2 H_3}{\partial y \partial \alpha} + \frac{1}{y}\frac{\partial H_3}{\partial \alpha} - \frac{1}{y} H_4 - \frac{\partial H_4}{\partial y} - \frac{\partial H_5}{\partial \alpha} + H_6 \right] T_1 + 1 = 0. \tag{D.14}$$

T_1 can be similarly solved by the method illustrated in Appendix C.

Supplementary material

Supplementary material associated with this article can be found, in the online version, at doi:10.1016/j.jmps.2019.103787.

References

Agrawal, H., Liu, L., Sharma, P., 2016. Revisiting the curvature-mediated interactions between proteins in biological membranes. Soft Matter 12 (43), 8907–8918.

Ahmadpoor, F., Sharma, P., 2016. Thermal fluctuations of vesicles and nonlinear curvature elasticity implications for size-dependent renormalized bending rigidity and vesicle size distribution. Soft Matter 12 (9), 2523–2536.

Arroyo, M., DeSimone, A., 2009. Relaxation dynamics of fluid membranes. Phys. Rev. E 79 (3), 31915.

Arroyo, M., Walani, N., Torres-Sánchez, A., Kaurin, D., 2018. Onsager's variational principle in soft matter: introduction and application to the dynamics of adsorption of proteins onto fluid membranes. In: The Role of Mechanics in the Study of Lipid Bilayers. Springer, pp. 287–332.

Di Leonardo, R., Keen, S., Ianni, F., Leach, J., Padgett, M., Ruocco, G., 2008. Hydrodynamic interactions in two dimensions. Phys. Rev. E 78 (3), 31406.

Doi, M., Edwards, S.F., 1988. The Theory of Polymer Dynamics, Vol. 73. Oxford university press.

Donev, A., Vanden-Eijnden, E., Garcia, A., Bell, J., 2010. On the accuracy of finite-volume schemes for fluctuating hydrodynamics. Comm. App. Math. Comp. Sci. 5 (2), 149–197.

Evans, L.C., 2010. Partial Differential Equations. American Mathematical Society.

Gillespie, D.T., 1991. Markov Processes: An Introduction for Physical Scientists. Elsevier.

Golestanian, R., Goulian, M., Kardar, M., 1996. Fluctuation-induced interactions between rods on a membrane. Phys. Rev. E 54 (6), 6725.

Granek, R., 1997. From semi-flexible polymers to membranes: anomalous diffusion and reptation. J. Phys. II 7 (12), 1761–1788.

Han, Y., Alsayed, A., Nobili, M., Yodh, A.G., 2009. Quasi-two-dimensional diffusion of single ellipsoids: aspect ratio and confinement effects. Phys. Rev. E 80 (1), 11403.

Han, Y., Alsayed, A., Nobili, M., Zhang, J., Lubensky, T.C., Yodh, A.G., 2006. Brownian motion of an ellipsoid. Science 314 (5799), 626–630.

Hanlumyuang, Y., Liu, L., Sharma, P., 2014. Revisiting the entropic force between fluctuating biological membranes. J. Mech. Phys. Solids 63, 179–186.

Hormel, T.T., Kurihara, S.Q., Brennan, M.K., Wozniak, M.C., Parthasarathy, R., 2014. Measuring lipid membrane viscosity using rotational and translational probe diffusion. Phys. Rev. Lett. 112 (18), 188101.

Huang, C., Yuan, H., Zhang, S., 2011. Coupled vesicle morphogenesis and domain organization. Appl. Phys. Lett. 98 (4), 43702.

Itô, S., et al., 1957. A boundary value problem of partial differential equations of parabolic type. Duke Math. J. 24 (3), 299–312.

Kahraman, O., Koch, P.D., Klug, W.S., Haselwandter, C.A., 2016. Architecture and function of mechanosensitive membrane protein lattices. Sci. Rep. 6, 19214.

Kim, K., Neu, J., Oster, G., 1998a. Curvature-mediated interactions between membrane proteins. Biophys. J. 75 (5), 2274–2291.

Kim, K., Neu, J., Oster, G., 1998b. Curvature-mediated interactions between membrane proteins. Biophys. J. 75 (5), 2274–2291.

Kwiecinski, J.A., Chapman, S.J., Goriely, A., 2019. Private communication.

Li, H., Lykotrafitis, G., 2015. Vesiculation of healthy and defective red blood cells. Phys. Rev. E 92 (1), 12715.

Liang, X., Purohit, P.K., 2016. A fluctuating elastic plate and a cell model for lipid membranes. J. Mech. Phys. Solids 90, 29–44.

Liang, X., Purohit, P.K., 2018. A method to compute elastic and entropic interactions of membrane inclusions. Extreme Mech. Lett. 18, 29–35.

Lin, H.-K., Zandi, R., Mohideen, U., Pryadko, L.P., 2011. Fluctuation-induced forces between inclusions in a fluid membrane under tension. Phys. Rev. Lett. 107 (22), 228104.

Lin, L.C.-L., Brown, F.L., 2004. Brownian dynamics in fourier space: membrane simulations over long length and time scales. Phys. Rev. Lett. 93 (25), 256001.

Lindgren, E.B., Derbenev, I.N., Khachatourian, A., Chan, H.-K., Stace, A.J., Besley, E., 2018. Electrostatic self-assembly: understanding the significance of the solvent. J. Chem. Theory Comput. 14 (2), 905–915.

Matthews, R., Likos, C.N., 2013. Dynamics of self-assembly of model viral capsids in the presence of a fluctuating membrane. J. Phys. Chem. B 117 (27), 8283–8292.

Müller, M.M., Deserno, M., 2010. Cell model approach to membrane mediated protein interactions. Prog. Theor. Phys. Suppl. 184, 351–363.

Öttinger, H.C., 1996. Stochastic processes, polymer dynamics, and fluid mechanics. In: Stochastic Processes in Polymeric Fluids. Springer, pp. 1–15.

Perrin, F., 1934. Mouvement brownien d'un ellipsoide-i. dispersion diélectrique pour des molécules ellipsoidales. J. Phys. Radium 5 (10), 497–511.

Perrin, F., 1936. Mouvement brownien d'un ellipsoide (ii). rotation libre et dépolarisation des fluorescences. translation et diffusion de molécules ellipsoidales. J. Phys. Radium 7 (1), 1–11.

Reynwar, B.J., Illya, G., Harmandaris, V.A., Müller, M.M., Kremer, K., Deserno, M., 2007a. Aggregation and vesiculation of membrane proteins by curvature–mediated interactions. Nature 447 (7143), 461.

Reynwar, B.J., Illya, G., Harmandaris, V.A., Müller, M.M., Kremer, K., Deserno, M., 2007b. Aggregation and vesiculation of membrane proteins by curvature–mediated interactions. Nature 447 (7143), 461.

Risken, H., 1996. Fokker-Planck equation. In: The Fokker-Planck Equation. Springer, pp. 63–95.

Pathria, R.K., Beale, P.D., 2011. Statistical Mechanics, third ed. Elsevier.

Rower, D., Padidar, M., Atzberger, P.J.. Surface fluctuating hydrodynamics methods for the drift-diffusion dynamics of particles and microstructures within curved fluid interfaces.

Ruiz-Herrero, T., Hagan, M.F., 2015. Simulations show that virus assembly and budding are facilitated by membrane microdomains. Biophys. J. 108 (3), 585–595.

Saffman, P., Delbrück, M., 1975. Brownian motion in biological membranes. Proc. Natl. Acad. Sci. 72 (8), 3111–3113.

Schweitzer, Y., Kozlov, M.M., 2015. Membrane-mediated interaction between strongly anisotropic protein scaffolds. PLoS Comput. Biol. 11 (2), e1004054.

Shnyrova, A.V., Ayllon, J., Mikhalyov, I.I., Villar, E., Zimmerberg, J., Frolov, V.A., 2007. Vesicle formation by self-assembly of membrane-bound matrix proteins into a fluidlike budding domain. J. Cell Biol. 179 (4), 627–633.

Tozzi, C., Walani, N., Arroyo, M., 2019. Out-of-equilibrium mechanochemistry and self-organization of fluid membranes interacting with curved proteins. New J. Phys.
Yolcu, C., Haussman, R.C., Deserno, M., 2014a. The effective field theory approach towards membrane-mediated interactions between particles. Adv Colloid Interface Sci 208, 89–109.
Yolcu, C., Haussman, R.C., Deserno, M., 2014b. The effective field theory approach towards membrane-mediated interactions between particles. Adv. Colloid Interface Sci. 208, 89–109.
Yolcu, C., Rothstein, I.Z., Deserno, M., 2011. Effective field theory approach to Casimir interactions on soft matter surfaces. EPL 96 (2), 20003.
Zhang, Y., Crothers, D.M., 2003. Statistical mechanics of sequence-dependent circular DNA and its application for DNA cyclization. Biophys. J. 84 (1), 136–153.